HHS Public Access

Author manuscript

Cell Rep. Author manuscript; available in PMC 2023 October 18.

Published in final edited form as:

Cell Rep. 2023 September 26; 42(9): 113029. doi:10.1016/j.celrep.2023.113029.

Lateral preoptic area glutamate neurons relay nociceptive information to the ventral tegmental area

David J. Barker[1,3,4], **Shiliang Zhang**[2,4], **Huiling Wang**[1], **David J. Estrin**[1], **Jorge Miranda-Barrientos**[1], **Bing Liu**[1], **Rucha J. Kulkarni**[1], **Junia Lara de Deus**[1], **Marisela Morales**[1,5,*]

[1]Integrative Neuroscience Branch, Neuronal Networks Section, National Institute on Drug Abuse Intramural Research Program, Baltimore, MD 21224, USA

[2]Confocal and Electron Microscopy Core, National Institute on Drug Abuse Intramural Research Program, Baltimore, MD 21224, USA

[3]Present address: Department of Psychology, Rutgers University, Piscataway, NJ 08854, USA

[4]These authors contributed equally

[5]Lead contact

SUMMARY

The ventral tegmental area (VTA) has been proposed to play a role in pain, but the brain structures modulating VTA activity in response to nociceptive stimuli remain unclear. Here, we demonstrate that the lateral preoptic area (LPO) glutamate neurons relay nociceptive information to the VTA. These LPO glutamatergic neurons synapsing on VTA neurons respond to nociceptive stimulation and conditioned stimuli predicting nociceptive stimulation and also mediate aversion. In contrast, LPO GABA neurons synapsing in the VTA mediate reward. By ultrastructural quantitative synaptic analysis, *ex vivo* electrophysiology, and functional neuroanatomy we identify a complex circuitry between LPO glutamatergic and GABAergic neurons and VTA dopaminergic, GABAergic, and glutamatergic neurons. We conclude that LPO glutamatergic neurons play a causal role in the processing of nociceptive stimuli and in relaying information about nociceptive stimuli. The pathway from LPO glutamatergic neurons to the VTA represents an unpredicted interface between peripheral nociceptive information and the limbic system.

In brief

*Correspondence: mmorales@intra.nida.nih.gov.

AUTHOR CONTRIBUTIONS

M.M. and D.J.B. conceptualized the project. D.J.B., H.W., and D.J.E. performed and/or analyzed data from optogenetic or fiber photometry behavioral studies. D.J.B., H.W., and B.L. performed and analyzed tracing and *in situ* hybridization studies. D.J.B. and S.Z. performed and/or analyzed the electron microscopy experiments. Viral injections were performed by D.J.B., H.W., and D.J.E. *Ex vivo* electrophysiology experiments were performed by J.M.-B and J.L.D. D.J.B. performed statistical analysis. D.J.B., S.Z., and M.M. wrote the manuscript with contributions from all coauthors.

DECLARATION OF INTERESTS

The authors declare no competing interests.

SUPPLEMENTAL INFORMATION

Supplemental information can be found online at https://doi.org/10.1016/j.celrep.2023.113029.

Barker et al. discover that a previously undefined population of lateral preoptic area glutamate neurons relays nociceptive information to the ventral tegmental area via the activation of ventral tegmental area GABA neurons.

Graphical Abstract

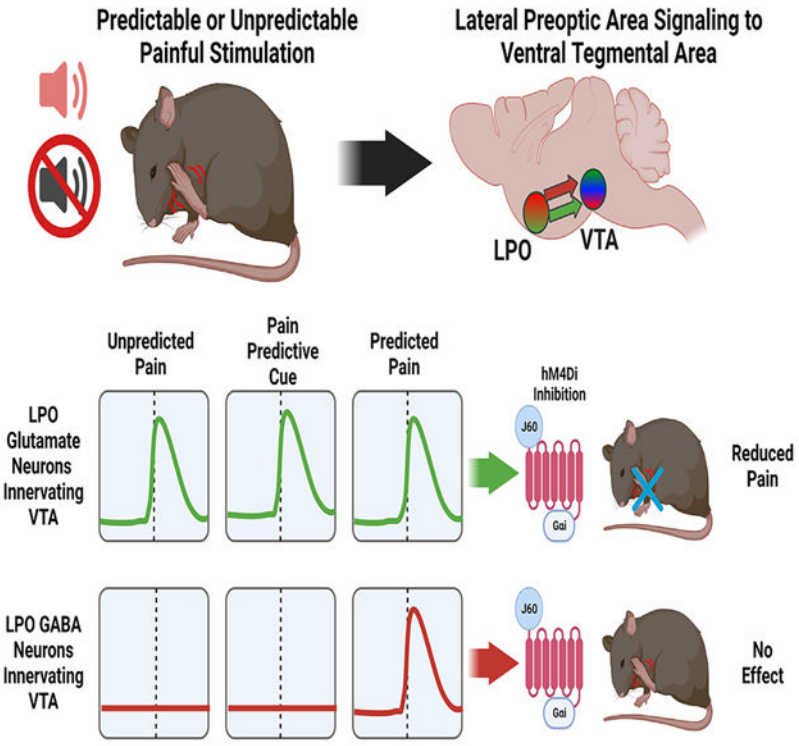

INTRODUCTION

Chronic pain is comorbid with several mental illnesses, including depression, anxiety, and substance-use disorders.[1,2] While nearly 30% of Americans live with some form of acute or chronic pain, only a fraction of them show susceptibility to mental illness.[2] Several studies have shown that the effect of pain on the brain may be cumulative, as the degree and frequency of pain experienced by an individual are correlated with the probability of developing mood disorders.[1] Given that a predictor of the susceptibility to mental illnesses such as depression and substance abuse is the development of negative emotional states,[3–8] this may explain in part the higher prevalence of mental illnesses such as anxiety disorders or depression in patients with chronic pain than in the population at large,[1] and these patients appear to experience pain more strongly.[9] Overall, these results indicate a complex relationship between chronic pain and mental illnesses and the need for having a better understanding on how pain affects brain structures that process emotion and mood.

The ventral tegmental area (VTA) is one of the brain structures proposed to play a role in pain, with specific roles in opioid-mediated signaling,[10] emotional processing,[11,12] mood disorders,[13,14] and the processing of nociceptive stimuli. The VTA is a highly heterogeneous midbrain structure, composed of dopamine neurons (expressing tyrosine hydroxylase [TH]), glutamate neurons (expressing vesicular glutamate transporter 2 [VGluT2]), and GABA neurons (expressing glutamic acid decarboxylase [GAD], for synthesis of GABA, and vesicular GABA transporter [VGaT]), as well as subtypes of neurons that release more than one of these neurotransmitters.[15,16] A role for VTA dopamine neurons in pain has been suggested from studies showing that pain—especially when chronic—causes an overall reduction in mesolimbic dopamine transmission[17] and that 6-hydroxydopamine lesions of VTA dopamine neurons attenuate the analgesic effects of morphine.[18,19] Further, pain relief has been linked to increases in dopamine release within the nucleus accumbens[20]; however, the release of dopamine in response to opioids is attenuated in response to chronic injury or inflammation.[21,22] In addition to dopamine neurons, VTA GABA neurons appear to play a role in nociceptive processing, as chronic neuropathic injury has been shown to cause increases in the VTA cellular expression of GAD and VGaT.[23] In addition to these molecular changes, chronic neuropathic injury increases the firing rate of VTA GABA neurons, decreases the firing rate for neighboring dopamine neurons, and increases negative affective behaviors in the rat.[23]

At present, it is unclear what different brain areas participate in regulating VTA neuronal activity related to pain. One unexamined pathway by which nociceptive information might reach and influence the VTA is through inputs from the lateral preoptic area (LPO). The LPO is a hypothalamic brain structure that heavily innervates the VTA[24] and receives direct inputs from the dorsal horn of the spinal cord[25–29]—an area containing nociceptors, pain-sensing neurons. The involvement of the LPO in nociceptive processing has been proposed based on results from several studies, including *in vivo* recordings in rodents showing an increase in the firing rate of a subset of LPO neurons in response to electric shocks or tail pinches.[30,31] In addition, noxious injections of formalin into the hindpaw of rats induce the release of excitatory amino acids (glutamate, arginine, and aspartate) within the LPO,[32] and injection of the proinflammatory cytokine IL-1β into the LPO produces hyperalgesia (increased sensitivity to nociceptive stimuli).[33]

Here, we applied a multidisciplinary approach to test the hypothesis that the LPO relays nociceptive information to the VTA and, in the process, identified a circuit from LPO glutamatergic neurons to VTA neurons that participates in processing nociceptive information.

RESULTS

LPO glutamate and LPO GABA neurons target the VTA, but LPO glutamate neurons relay nociceptive information to VTA

While the LPO has been traditionally considered a dominantly GABAergic structure, prior anatomical evidence suggests that the LPO provides a large glutamatergic input to the VTA.[34] To quantitatively determine the nature of the LPO neurons innervating the VTA, we delivered the retrograde tract tracer FluoroGold (FG) into the VTA and found that

FG delivery resulted in major FG labeling in the preoptic area and some labeling in adjacent structures (Figures S1A–S1C and S1F–S1I). By *in situ* hybridization phenotypic characterization of LPO FG neurons (Figure S1D), we found that as many as 42.3% ± 2.4% of FG-positive LPO neurons expressed VGluT2 mRNA (195/458 neurons) (Figures S1D, S1E, and S1H–S1I), and 65.4% ± 3.5% expressed VGaT mRNA (244/383 neurons) (Figures S1D, S1E, S1H, and S1I). These data indicate that, within the basal forebrain, the LPO provides a major glutamatergic and GABAergic input to the VTA.

LPO neurons are part of a continuum of neurons in the hypothalamus that receive input from the dorsal horn of the spinal cord.[25–29] Thus, we hypothesized that either LPO glutamate (LPO-VGluT2) or LPO GABA (LPO-VGaT) neurons provide a source of nociceptive input to the VTA. To test this hypothesis, we injected a retrograde viral vector, AAV6, encoding channelrhodopsin (ChR2) into the sciatic nerve of *vglut2:cre* or *vgat:cre* mice, to allow the photostimulation of peripheral nociceptors via stimulation of free nerve endings in the paw.[35–37] Into the VTA of the same mice, we injected the retrograde Cre-dependent HSV-hEF1α-LS1L-GCaMP6s viral vector to express GCaMP6s in either LPO-VGluT2 or LPO-VGaT neurons targeting the VTA. We implanted an optic fiber over the LPO to record Ca^{2+} responses by fiber photometry across photostimulations of the rear hindpaw expressing ChR2 in the sciatic nerve (Figures 1A and S2A). Next, we determined the effects of injections of morphine (5 mg/kg) on paw withdrawal responses and neuronal activity of VTA-projecting LPO-GluT2 or LPO-VGaT neurons.

We observed that photostimulation of the paw resulted in rapid paw withdrawal, as well as shaking or licking of the paw (nocifensive behaviors) and found that morphine (5 mg/kg) significantly increased the latency for paw withdrawal in both *vglut2: cre* and *vgat:cre* mice (Figure 1B). By fiber photometry Ca^{2+} imaging, we observed that LPO-VGluT2 neurons innervating the VTA exhibited a significant increase in Ca^{2+} activity in response to photostimulation of the hindpaw (Figure 1C), the magnitude of which was significantly correlated with paw withdrawal latency (Figure S3A). In addition to responses to photostimulation, we observed that some mice exhibited *anticipatory*, prestimulation responses while the laser was being positioned below the hindpaw. In common with the effect on behavioral responses, Ca^{2+} responses were blocked by morphine (5 mg/kg) (Figure 1C). In contrast, *vglut2:cre* mice whose hindpaw was injected with an AAV6 encoding a yellow fluorescent protein (eYFP) did not exhibit rapid nocifensive responses to the laser and exhibited a much weaker Ca^{2+} response at the time of paw withdrawal (Figures S3B and S3C). Moreover, LPO-VGaT neurons innervating VTA neurons did not show any increase in Ca^{2+} activity at the time of photostimulation. The activity of LPO-VGaT neurons innervating the VTA was also unaffected by the administration of morphine (Figure 1D).

Conditioned responses to nociceptive stimuli by LPO glutamate and LPO GABA neurons targeting the VTA

As indicated above, during nociceptive paw photostimulation, we observed that a subset of mice showed anticipatory increases in Ca^{2+} signaling just prior to laser stimulation in response to audiovisual cues while the laser was being adjusted to target the hindpaw. Thus, we next evaluated the possible involvement of LPO-VGluT2 or LPO-VGaT neurons

innervating the VTA in conditioned responses to nociceptive stimuli in mice expressing ChR2 in the sciatic nerve. For this experiment, we paired a tone with the delivery of blue light via a light-emitting diode (LED) grid in the floor of the test chamber to stimulate peripheral nociceptors via stimulation of ChR2-expressing free nerve endings in the paw and recorded Ca^{2+} activity in LPO-VGluT2 and LPO-VGaT neurons innervating the VTA (Figure 2A). We observed increases in Ca^{2+} activity in LPO-VGluT2, but not LPO-VGaT, neurons innervating the VTA in response to a tone predicting hindpaw photostimulation and a second, greater peak in Ca^{2+} activity at the time of the paw stimulation (Figure 2B). Responses to the cue were absent upon the first (naive) tone exposure, but rapidly developed over the course of the first conditioning session (Figure S3D). Moreover, both types of responses of LPO-VGluT2 neurons innervating the VTA were consistent across all conditioning sessions, and the responses to the cue were also present during a photostimulation-free test session. In contrast to the lack of increase in Ca^{2+} activity at the time of spontaneous paw stimulation by LPO-VGaT neurons innervating the VTA, we observed a small increase in Ca^{2+} activity at the time of predictable hindpaw stimulation by VTA-projecting LPO-VGaT neurons (Figure 2C). Collectively, these findings indicate that, while both LPO-VGluT2 and LPO-VGaT neurons targeting the VTA participate in signaling a conditioned pain response, the LPO-VGluT2 neurons appear to have a strong response to nociceptive stimuli.

VTA activation of LPO glutamate inputs is aversive

Recorded Ca^{2+} responses indicated that LPO-VGluT2 neurons targeting the VTA were activated by the stimulation of peripheral nociceptors, while LPO-VGaT neurons targeting the VTA were responsive only when nociceptive stimuli became predictable. To determine whether LPO-VGluT2 or LPO-VGaT neurons targeting the VTA participate in predicting and signaling the aversive aspects of nociceptive stimuli, we injected into the LPO of *vglut2:cre* or *vgat:cre* mice either a Cre-dependent adeno-associated viral vector encoding ChR2 tethered to eYFP (AAV-DIO-ChR2-eYFP; VGluT2-LPO$^{ChR2\text{-}eYFP}$ or VGaT-LPO$^{ChR2\text{-}eYFP}$ mice) or eYFP alone as a control (AAV-DIO-eYFP; VGluT2-LPO^{eYFP} or VGaT-LPO^{eYFP} mice) and placed an optic fiber over the VTA for the photostimulation of VTA fibers from LPO-VGluT2 or LPO-VGaT neurons (Figures 3A and S2B). We tested mice in a three-chamber apparatus with two chambers (one paired with laser stimulation) and one connecting chamber. Continuous trains of 20 Hz photostimulation were delivered when mice entered the photostimulation-paired chamber and terminated when mice exited the chamber (Figure 3B).

In the presence of VTA photostimulation, VGluT2-LPO$^{ChR2\text{-}eYFP}$ mice avoided the chamber that was paired with laser stimulation, spending more time in the photostimulation-unpaired chamber. These VGluT2-LPO$^{ChR2\text{-}eYFP}$ mice also exhibited a conditioned avoidance response when tested in the absence of VTA stimulation and reliably reversed their behavior when stimulation in the paired and unpaired compartments was switched. Responses to the laser stimulation were consistent with conventional escape-avoidance behaviors in the mouse and did not produce any deleterious effects. The control VGluT2-LPO^{eYFP} mice exhibited neither a preference for nor an aversion to the photostimulation-paired chamber. Overall, these results showed a role for LPO-VGluT2

neurons innervating the VTA in signaling aversive, nociceptive information (Figure 3C). In contrast, VGaT-LPO$^{ChR2\text{-}eYFP}$ mice exhibited a preference for the chamber paired with VTA photostimulation, and switching the photostimulation-paired and unpaired compartments readily reversed the preference for the photostimulation-paired chamber. Prolonged experience with photostimulation resulted in a conditioned preference for the photostimulation-paired chamber during the stimulation-free test that followed reversal training. The control VGaT-LPO^{eYFP} mice did not show any consistent preferences for the stimulation-paired chamber (Figure 3D). These results indicate that activation of LPO GABA projections to the VTA was reinforcing.

LPO glutamate inputs to the VTA signal aversion through a mechanism independent of VTA glutamatergic neurons

After establishing that VTA photostimulation of LPO-VGluT2 axons was aversive, we next determined the extent to which activation of these inputs induced the expression of c-Fos (a marker of neuronal activation) in the different classes of VTA neurons. For these anatomical studies, brains from a separate group of VGluT2-LPO$^{ChR2\text{-}eYFP}$ and VGluT2-LPO^{eYFP} mice were collected 2 h after aversion testing. We detected 2.6 times more c-Fos neurons in the VTA of ChR2-eYFP mice (359.7 ± 11.3 neurons; 1,619 total counted c-Fos neurons) than in the VTA of eYFP mice (206.0 ± 16.8 neurons; 618 total counted c-Fos neurons; Figures 4A–4F and Table S1).

Within the ChR2-eYFP mice, we found that c-Fos was differentially induced in the major classes of VTA neurons: ≈45% expressed VGluT2 mRNA (735 c-Fos-VgluT2 neurons/1,619 c-Fos neurons), ≈20% expressed VGaT mRNA (323 c-Fos-VGaT neurons/1,619 c-Fos neurons), ≈16% expressed VGluT2 mRNA and TH (256 c-Fos-VGluT2-TH neurons/1,619 c-Fos neurons), ≈8% expressed VGluT2 and VGaT mRNAs (136 c-Fos-VGluT2-VGaT neurons/1,619 c-Fos neurons), and ≈2% expressed TH (25 c-Fos-TH neurons/1,619 c-Fos neurons). These findings indicate that the VTA release of glutamate from LPO inputs induced c-Fos in several VTA cell types, with some of the strongest increases in neurons expressing VGluT2 mRNA, VGluT2 mRNA and TH, or VGaT mRNA.

Based on the number of activated VTA cell types that expressed VGluT2 mRNA, we hypothesized that LPO glutamate inputs might signal aversion through the activation of VTA glutamate or glutamate cotransmitting neurons. To test this hypothesis, we injected the LPO of *vglut2:cre* mice with an AAV-DIO-ChR2-eYFP for the stimulation of LPO-VGluT2 fibers in the VTA. In the VTA of the same mice, we then injected a Cre-dependent caspase viral vector (AAV-FLEX-Casp3) to selectively ablate VTA neurons expressing (or coexpressing) *vglut2* before implanting an optic fiber for the VTA photostimulation of LPO-VGluT2 fibers (Figure 4G). The VTA injection of caspase-3 resulted in an ≈92% reduction in VTA VGluT2-expressing neurons (Figure 4H), but this selective ablation did not affect the avoidance of the chamber paired with VTA photostimulation of LPO-VGluT2 fibers (Figure 4I). These findings indicate that LPO glutamate inputs to the VTA are sufficient to activate VTA glutamate neurons, but that VTA glutamate neurons are not necessary for the expression of aversion observed following the activation of this pathway.

LPO inputs provide differential excitatory or inhibitory inputs to VTA TH, VGluT2, and VGaT neurons

Given the glutamatergic and GABAergic nature of LPO inputs to the VTA and the VTA cellular heterogeneity, we next applied immunofluorescence, immunoelectron microscopy, and *ex vivo* electrophysiology to better characterize the nature of the synapses established between LPO glutamatergic and GABAergic and VTA VGluT2, VGaT, and TH neurons.

For confocal and electron microscopy, we tagged LPO neurons by injecting an AAV viral vector tethered to mCherry (AAV-CaMKIIa-ChR2-mCherry) into the LPO of *vglut2:cre* or *vgat:cre* mice to express ChR2 in LPO neurons and axons. In the VTA of these LPO-injected mice, we injected a Cre-dependent AAV-DIO-eYFP for *in vivo* labeling of TH, VGluT2, or VGaT neurons (Figures 5A, 5E, S4A, S5A, S5D, S6A, and S7A). In the VTA of dual-injected *vglut2:cre* mice, we determined the nature of the LPO inputs synapsing on VTA-TH (identified by TH immunolabeling) and VTA-VGluT2 neurons (identified by eYFP expression). By VTA immunolabeling (mCherry, TH, and eYFP) and confocal microscopy, we detected LPO axons (mCherry) within the medial and lateral aspects of the ventral VTA (Figures 5B and S4B). These LPO mCherry axons were intermixed with VTA neurons expressing TH (TH-only neurons), eYFP (VGluT2-only neurons) or both (TH-eYFP; TH-VGluT2 neurons). Consistent with our prior quantifications of VTA TH and VGluT2 distributions,[38,39] we observed by confocal microscopy TH-only neurons in the lateral VTA, some dual TH-eYFP neurons in the medial and mediolateral VTA, and some eYFP-only in the medial and mediolateral VTA (Figure S4). We found that LPO mCherry axon terminals expressing VGluT2 established contacts on primary dendrites of TH-only, dual TH-VGluT2, and VGluT2-only neurons (Figures 5C and S4), but infrequently on the soma of VTA neurons. By VTA triple immunoelectron microscopy, we determined that LPO mCherry-VGluT2 axon terminals established asymmetric (putative excitatory) synapses with TH and VGluT2 dendrites (Figures 5D and S6F). In the VTA of dual-injected *vgat:cre* mice, we determined the nature of the LPO inputs synapsing specifically on VTA-VGaT neurons (identified by eYFP expression) (Figure 5E). By VTA triple immunolabeling (mCherry, TH, and eYFP) and confocal microscopy, we detected LPO mCherry axons intermixed with VTA neurons expressing either TH or eYFP (VGaT neurons) (Figure 5F). We found that LPO mCherry axon terminals expressing VGluT2 infrequently contacted the soma of VTA-VGaT neurons, and they mainly contacted primary dendrites of VTA-VGaT neurons (Figure 5G). By VTA triple immunoelectron microscopy, the axon terminals of LPO-VGluT2 neurons established asymmetric synapses on VTA-VGaT primary (Figure 5H) and secondary dendrites (Figure S7C). In the same experiment, we detected LPO-VGaT axon terminals establishing synapses on VTA neurons. In the VTA of dual-injected *vglut2:cre* mice, by VTA triple immunolabeling and confocal microscopy, we found that LPO mCherry axon terminals expressing VGaT established multiple contacts on the soma and dendrites of TH-only, dual TH-VGluT2, and VGluT2-only neurons (Figure S5B). By VTA triple immunoelectron microscopy, we determined that LPO mCherry terminals coexpressing VGaT established multiple symmetric (putative inhibitory) synapses on the soma of both TH and VGluT2 neurons (Figure S5C), as well as with TH or VGluT2 primary dendrites (Figures S6B–S6E). In the VTA of dual-injected *vgat:cre* mice, LPO mCherry axon terminals expressing VGaT established multiple contacts on the soma of

VGaT neurons lacking TH immunolabeling (Figure S5E). The LPO mCherry-VGaT axon terminals also contacted VGaT dendrites. By VTA triple immunoelectron microscopy, we determined that LPO mCherry terminals coexpressing VGaT established multiple symmetric synapses on the soma or dendrites of VGaT neurons (Figures S5F and S7B).

By serial section electron microscopy, we quantified and compared the numbers of synapses established by LPO-VGaT or LPO-VGluT2 axon terminals on VTA-TH, VTA-GluT2, or VTA-VGaT neurons located in the lateral or medial VTA from three dual-injected *vglut2:cre* mice and three dual-injected *vgat:cre* mice (Tables S2 and S3). We found that the total number of synapses between LPO axon terminals from LPO-VGluT2 neurons and VTA neurons were comparable in the medial (49.9%, 524/1,046 synapses) and lateral (50.1%, 522/1,046 synapses) VTA. In contrast, we determined that the total numbers of synapses between LPO axon terminals from LPO-VGaT neurons making synapses on VTA neurons were higher in the medial (56.4%, 660/1,171 synapses) than the lateral (43.6%, 511/1,171 synapses) VTA. These findings indicate that, while the synapses established by LPO-VGluT2 neurons within the VTA were evenly distributed within the VTA, the synapses established by LPO-VGaT neurons had a topographic mediolateral decreasing distribution.

Next, we determined the frequency and postsynaptic phenotype of VTA neurons establishing synapses with LPO axon terminals and found that axon terminals from LPO-VGluT2 neurons differentially established synapses on dendrites of the distinct classes of VTA neurons (Table S2 and Figure S8A) Within the medial VTA, we found that LPO-VGluT2 neurons synapsed with similar frequencies on dendrites of VGluT2 (32.0% ± 4.8%, 61/190 synapses) or VGaT neurons (31.8% ± 3.8%, 68/ 220 synapses) and with lesser frequency on dendrites of TH neurons (27.3% ± 5.0%, 31/114 synapses). In contrast, within the lateral VTA, the LPO-VGluT2 neurons preferentially synapse on dendrites of VGaT neurons (39.1% ± 4.2%, 65/153 synapses) and with comparable frequencies on dendrites of TH (32.4% ± 2.7%, 52/162 synapses) and VGluT2 neurons (31.7% ± 1.9%, 66/207 synapses). In common with synapses by LPO-VGluT2 neurons, we found that LPO-VGaT neurons differentially established synapses on dendrites of the distinct classes of VTA neurons. Within the medial VTA, we found that LPO-VGaT neurons more often synapsed on dendrites of VGluT2 neurons (38.0% ± 7.6%, 102/263), followed by synapses on dendrites of TH (33.8% ± 5.4%, 69/208 synapses) or VGaT (24.6% ± 2.8%, 50/189 synapses) neurons. In contrast, within the lateral VTA, LPO-VGaT neurons synapsed with comparable frequencies on dendrites of TH (48.4% ± 5.6%, 103/205 synapses) or VGluT2 (45.6% ± 6.5%, 68/154 synapses) neurons and with lowest frequency on dendrites of VGaT neurons (46/152 synapses = 30.7% ± 3.3%).

In addition to postsynaptic dendrites, we noticed that LPO neurons established synapses on the soma of VTA neurons (Table S3 and Figure S8B). Within the medial VTA, we found that LPO-VGluT2 neurons preferentially synapsed on the soma of VGaT neurons (28.4% ± 7.6%, 23/83 synapses), followed with comparable frequency on the soma of TH (20.2% ± 6.6%, 13/70 synapses) and VGluT2 neurons (19.7% ± 3.7%, 21/113 synapses). In contrast, within the lateral VTA, LPO-VGluT2 neurons preferentially synapsed on the soma of TH neurons (16.0% ± 5.8%, 13/78 synapses), followed by synapses on the soma of VGaT neurons (12.8% ± 3.5%, 7/54 synapses), and with lowest frequency on the soma

of VGluT2 neurons (10.9% ± 6.4%, 6/53 synapses). In common with synapses by LPO-VGluT2 neurons, we found that LPO-VGaT neurons differentially established synapses on the soma of the distinct classes of VTA neurons. Within the medial VTA, we determined that LPO-VGaT neurons synapsed with comparable frequencies on the soma of TH (29.9% ± 12.0%, 24/70 synapses), VGluT2 (25.1% ± 12.6%, 18/66 synapses), or VGaT (24.9% ± 12.6%, 15/62 synapses) neurons. In contrast, within the lateral VTA, LPO-VGaT neurons preferentially synapsed on the soma of VGaT neurons (58.0% ± 0.7%, 51/88 synapses), followed by synapses on the soma of TH neurons (46.8% ± 15.9%, 32/68 synapses), and with the lowest frequency on the soma of VGluT2 neurons (30.3% ± 15.6%, 30/68 synapses).

For electrophysiological studies, we tagged LPO neurons and their axons by injecting an AAV viral vector tethered to mCherry (AAV-CaMKIIa-ChR2-mCherry) into the LPO of *th:cre*, *vglut2:cre*, or *vgat:cre* mice. In the VTA of these LPO-injected mice, we injected a Cre-dependent AAV-DIO-eYFP for *in vivo* labeling of TH, VgluT2, or VGaT neurons (Figure 6A). By slice electrophysiology, we found that VTA photoactivation of LPO inputs induced excitatory postsynaptic currents (EPSCs) in nearly a third of the recorded TH neurons (7/20 neurons; amplitude from −11.6 to −130.1 pA; mean = −54.0 pA; 3/6 mice) and inhibitory postsynaptic currents (IPSCs) in a few TH neurons (3/20 neurons; amplitude from 18.0 to 191.7 pA; mean = 76.8 pA; 2/6 mice) and induced both EPSCs and IPSCs in half of the recorded TH neurons (10/20 neurons; EPSC amplitude from −5.0 to −63.0 pA, mean = −33.6 pA, and IPSC amplitude from 17.9 to 212.4 pA, mean = 152.7 pA; 4/6 mice) (Figures 6B–6F). From recordings of VTA-VGluT2 neurons we detected in less than half of them EPSCs (6/15 neurons; amplitude from −6.3 to −77.4 pA; mean = −31.3 pA; 5/8 mice), infrequently IPSCs (2/15 neurons, amplitude from 47 to 80.1 pA; mean = 63.6 pA; 2/8 mice), and both EPSCs and IPSCs in approximately half of the recorded VGluT2 neurons (7/15 neurons; EPSC amplitude from −9.8 to −55.5 pA; mean = −37.1 pA, and IPSC amplitude from 5.5 to 171.8 pA; mean = 94.4 pA; 5/8 mice) (Figures 6B–6F). In contrast to VTA-TH and VTA-VGluT2 neurons, we found that VTA photoactivation of LPO inputs infrequently induced EPSCs in VTA-VGaT neurons (2/23 neurons; amplitude from −57.2 to −197.6 pA; mean = −127.4 pA; 2/8 mice), induced IPSCs in a third of VTA-VGaT neurons (6/23 neurons; amplitude from 11.9 to 1273.2 pA; mean = 508.7 pA; 3/6 mice), and frequently induced both EPSCs and IPSCs in more than half of VGaT recorded neurons (15/23 neurons, EPSC amplitude from −9.2 to −192.9 pA, mean = −93.9 pA, and IPSC amplitude from 79.2 to 1227.2 pA, mean = 518.3 pA; 8 mice) (Figures 6B–6F). Collectively, these results indicate that LPO glutamatergic and LPO GABAergic neurons differentially provided to VTA-VGluT2, VTA-TH, and VTA-VGaT neurons independent excitatory and independent inhibitory as well as converging excitatory and inhibitory inputs.

To determine the strength of LPO glutamate and GABA inputs to the different types of VTA neurons, we compared the magnitude of EPSCs and IPSCs in VTA-TH, VTA-VGluT2, and VTA-VGaT neurons in response to VTA photoactivation of LPO inputs. We found that EPSCs recorded at −60 mV in VTA-VGaT neurons were higher in magnitude than those recorded in VTA-TH and VTA-VGluT2 neurons (−41.3 ± 9.5 pA for VTA-TH, 17 neurons/6 mice; 34.5 ± 8.6 pA for VGluT2 neurons, 14 neurons/8 mice; and −95.5 ± 25.6 pA for VTA-VGaT neurons, 17 neurons/8 mice) (Figure 6C). In common with the

EPSC results, IPSCs recorded at 0 mV in VTA-VGaT neurons were higher than IPSCs recorded in VTA-TH and VTA-VGluT2 neurons (VTA-TH, 131.0 ± 69.0 pA, 14 neurons/6 mice; VTA-VGluT2, 87.5 ± 38.6 pA, 9 neurons/8 mice; and VTA-VGaT, 513.5 ± 79.9 pA, 21 neurons/8 mice) (Figure 6E). After confirming that LPO excitatory inputs to the VTA were monosynaptic (Figures 6G and 6H), we next performed current-clamp recordings and analyzed the changes in membrane potential and neuronal activity produced by convergent LPO inputs. We discovered that photoactivating LPO inputs to the VTA produced action potentials in TH neurons (five TH neurons, two mice) (Figure 6I). In contrast, we observed that this same photoactivation produced a pause in the firing of VTA GABA neurons (four neurons, two mice) (Figure 6I). In the case of VTA VGluT2 neurons, we observed that photoactivation depolarized the neurons, but failed to reach the threshold to drive action potentials (five VGluT2 neurons, three mice) (Figure 6I). Combined, these results raise the possibility that the simultaneous release of LPO glutamate and GABA in the VTA would result in inhibition of VTA GABA neurons and activation of dopamine neurons. The present results demonstrate the complex monosynaptic connectivity between both LPO-VGluT2 and LPO-VGaT neurons and the different classes of VTA neurons. Collectively, the results from c-Fos expression, electrophysiology, and quantitative immunoelectron microscopy indicate that the selective VTA release of glutamate from LPO inputs would result in the activation of VTA glutamate and GABA neurons. However, our caspase genetic lesions (Figure 4) also demonstrate that VTA neurons expressing or coexpressing VGluT2 are not required for signaling aversion. Thus, we infer that LPO-VGluT2 neurons are likely to signal nociceptive information and aversion via VTA GABA neurons.

LPO glutamate inputs to the VTA participate in the expression of pain

To establish whether there is a causal role for VTA-projecting LPO-VGluT2 or LPO-VGaT neurons in the modulation of nocifensive responses, we targeted LPO → VTA glutamate and GABA neurons for chemogenetic inhibition during the formalin footpad test by VTA injection of the retrograde HSV encoding a Cre-dependent hM4Di DREADD (inhibitory designer receptor exclusively activated by designer drugs). Over the LPO of these same mice, we implanted a cannula for the delivery of the DREADD agonist J60 or artificial cerebrospinal fluid (aCSF) as a control (Figure 7A). We measured nocifensive licking in response to a hindpaw injection of formalin for mice injected with J60 or aCSF and found that chemogenetic inhibition of VTA-projecting LPO glutamate neurons by J60 reduced nocifensive licking responses in phase II (but not phase I) of the formalin test (Figures 7B and 7C). In contrast, inhibiting VTA-projecting LPO GABA neurons had no effect on nocifensive licking in either phase of the formalin test (Figures 7D and 7E).

Given that our optogenetic studies indicated that activation of LPO GABA neurons was rewarding, we designed a task that would allow us to examine licking responses (comparable to those measured in the formalin task) for a sucrose reward, both before and after the intracranial delivery of J60 or aCSF. Consistent with a role in reward processing, we observed that the circuit-specific inhibition of VTA-projecting LPO-GABA neurons did produce a reduction in licking responses for sucrose (Figure 7F).

DISCUSSION

The VTA has been implicated in different aspects of pain, and we now provide converging evidence indicating that LPO inputs to the VTA play a role in the processing of nociceptive stimuli. We found that, while both LPO GABA and LPO glutamate neurons innervate the VTA, the LPO glutamate neurons were activated in response to nociceptive stimulation of dorsal root ganglion neurons. Further, the LPO glutamate neurons that target the VTA were activated by an auditory cue predicting nociceptive stimulation of the paw. In contrast, the LPO GABA neurons that target the VTA were not activated by spontaneous stimulation of the paw but were mildly activated at the time of a predictable nociceptive stimulus. We found that LPO glutamate neurons innervating the VTA play a role in aversive conditioning and the LPO GABA neurons innervating the VTA play a role in reward. From this, we infer that, while LPO glutamate neurons innervating the VTA are involved in signaling aversive, nociceptive information, the LPO GABA neurons innervating the VTA are involved in mitigating the aversiveness of nociceptive stimuli when they become predictable. We determined that different classes of VTA neurons established excitatory synapses with axons from LPO glutamate neurons, but activation of LPO glutamate inputs to the VTA excited mainly VTA glutamate and GABA neurons, and we found that LPO glutamate neurons signal aversion in the VTA through a mechanism that does not appear to require VTA glutamatergic neurons. We conclude that the activity of VTA neurons during the processing of nociceptive stimuli is under the control of excitatory inputs from LPO glutamate neurons that signal the presence of nociceptive stimuli or conditioned stimuli predicting them. Moreover, having demonstrated that VTA glutamate neurons are not required for the signaling of aversion, we suggest that the aversion associated with nociceptive signaling by LPO glutamate neurons likely occurs via VTA GABA neurons. These LPO glutamate neurons synapsing on VTA neurons represent an interface between the processing of peripheral nociceptive information and the limbic system.

Based on the synaptic features between the LPO glutamate neurons and the VTA neurons, we infer that the signaling of aversive stimuli relayed by LPO glutamate neurons to the VTA may involve distinct neuron populations that participate in specific aversive pathways. Given the detection of synapses between LPO glutamatergic inputs and VTA GABA neurons, as well as the detection of c-Fos in a population of GABA neurons in response to VTA glutamate release from LPO axons, we suggest that excitatory inputs from the LPO result in the postsynaptic activation of VTA GABA neurons and the indirect signaling of aversion by inhibiting VTA dopamine neurons.[40] Regarding the observation of synapses between LPO glutamate neurons and dopamine neurons, and the detection of c-Fos in a subset of TH neurons coexpressing VGluT2 in response to VTA glutamate release from LPO axons, we suggest that glutamate release from LPO glutamate neurons activates VTA dopamine-glutamate neurons and may in part account for the recorded activation of some VTA dopamine neurons in response to aversive stimuli, which we and others have previously reported.[41–43] Furthermore, we showed that LPO glutamate neurons synapse on VTA glutamate neurons and demonstrated that VTA glutamate release from LPO axons preferentially induced c-Fos expression in medial VTA glutamate-only neurons. While it is known that a subset of VTA glutamate neurons participate in aversion via projections to the

lateral habenula[44] or nucleus accumbens parvalbumin interneurons,[45] we demonstrate here that VTA glutamate neurons are not required for the signaling of aversion in the LPO → VTA pathway.

Beyond the role of LPO glutamate inputs to the VTA in aversion and nociceptive signaling, we found that activation of LPO GABA terminals in the VTA induced a place preference. The potential pathways supporting such reward might involve LPO GABA inputs establishing more prominent synapses in the lateral VTA on the dendrites of glutamate neurons, dendrites and soma of dopamine neurons, and soma of GABA neurons. We had previously shown that a subset of VTA glutamatergic neurons plays a role in reward by establishing excitatory synapses on neighboring dopamine neurons,[46] and other subsets of VTA glutamatergic neurons play a role in aversion by establishing synapses in lateral habenula glutamatergic neurons[44] or synapses on parvalbumin neurons in the nucleus accumbens.[45] Thus, there is the possibility that LPO GABA neurons produce reward by inhibiting VTA glutamatergic projection neurons that signal aversion. Another possible pathway participating in reward might involve the inhibition of lateral VTA dopamine neurons that participate in aversion signaling.[42,47] Finally, the observation that LPO GABA neurons established multiple synapses with high frequency on dendrites and soma of lateral VTA GABA neurons raises the possibility that LPO GABA neurons signal reward by inhibiting VTA GABA neurons that normally exert inhibitory control over neighboring dopamine neurons. Overall, the ultrastructural synaptic findings together with *in vivo* recordings and behavior indicate that subsets of LPO neurons relay aversion, reward, or conditioned pain responses to the VTA throughout complex synaptic interactions with select neurons distributed across the medial or lateral VTA.

The VTA in pain and aversion

The VTA has been implicated in pain, but the pathways involved in this processing and the exact role of the VTA in pain remain to be determined. Consistent among studies on the VTA and pain is the observation that pain causes a reduction in both the activity of dopamine neurons and the release of dopamine.[17,20–23] In addition, chronic injury seems to produce an increase in VTA GABA activity,[23] while antinociceptive effects can be produced by the inhibition of GABA neurons in the caudal VTA or the tail of the VTA (rostromedial tegmental nucleus),[48] which in turn control dopamine neurons. Here we provide evidence for an LPO-to-VTA pathway that drove several of the responses that have been observed in VTA neurons in association with pain. We found that LPO glutamate neurons were rapidly activated by a nociceptive stimulus and provided a strong synaptic input to the different classes of VTA neurons and that the VTA-specific release of glutamate from LPO glutamate neurons was aversive. These LPO glutamate neurons establish synapses with dopamine, GABA, and glutamate neurons across the entire mediolateral span of the VTA. However, we determined that LPO glutamate neurons established synapses more frequently on medial VTA with dendrites and soma of GABA neurons and dendrites of glutamate neurons. When considering the current anatomical and functional data alongside our prior work showing that both VTA glutamate- and VTA GABA-releasing neurons increase their activity in response to foot shock and their cues predicting it,[41] we propose that LPO glutamatergic neurons signal the aversive properties of pain primarily through the activation of VTA

GABA neurons. LPO GABA neurons also provide a strong synaptic input onto VTA GABA neurons (by synapsing on their soma and primary dendrites), but in contrast to the effects of LPO glutamate release in the VTA, the release of LPO GABA into the VTA is reinforcing. Based on the synaptic connectivity established by LPO GABA neurons with each type of VTA neuron (Figures 5 and 6), it is likely that the VTA GABA neurons targeted by LPO GABA neurons are those that establish synapses with neighboring dopamine neurons. Thus, we suggest that the rewarding effects of VTA GABA release in reward are mediated, in part, by LPO GABA neurons providing inhibitory control of those VTA GABA neurons that synapse on dopamine neurons (LPO GABA neurons → VTA GABA neurons → VTA dopamine neurons → reward). In the context of pain, LPO GABA neurons could therefore support the release of dopamine that has been observed during pain relief.[20]

The VTA is well known for predicting the value of both rewarding[49] and aversive stimuli.[47] Moreover, the ability to predict aversive stimuli has been shown to help mitigate the corresponding stress response.[50–52] The critical role of aversive stimulus prediction has been observed in both human and animal studies showing preference for predictable aversive stimuli.[53,54] Thus, predictable noxious stimuli are preferred over those that are unpredictable,[55] and the ability to predict and potentially avoid a noxious or painful stimulus reduces the corresponding emotional response,[56] while also resulting in the release of dopamine.[57] Here we have demonstrated that a positively reinforcing signal from the LPO → VTA becomes active when a noxious stimulus becomes predictable. Further, we demonstrate mechanistically by *ex vivo* electrophysiology that the simultaneous activation of LPO glutamatergic and GABAergic inputs to the VTA results in the inhibition of VTA GABA neurons and the net activation of VTA dopamine neurons. Thus, the competition between LPO glutamate and GABA neurons on the VTA may be critically important for the qualitative perception of painful stimuli.

Limitations of the study

While we demonstrated that the LPO represents an important interface between peripheral nociceptive information and the limbic system, further work will be needed to determine how nociceptive information arrives at the LPO, as well as how neurons in the LPO → VTA pathway act to modulate the expression of pain responses. One specific limitation of the present study was our inability to specifically verify that LPO glutamate neurons induced action potentials in VTA GABA neurons to facilitate responses to nociceptive stimuli (although c-Fos and EPSCs were observed). In addition, our conditioning experiments suggest that the LPO may play an important role in affective pain, but our evaluation of this remained limited. Thus, future work should focus on clarifying the role of the LPO in affective pain and the specific connectivity supporting these responses.

STAR★METHODS

RESOURCE AVAILABILITY

Lead contact—Further information and requests for resources and reagents should be directed to and will be fulfilled by the lead contact, Marisela Morales at mmorales@intra.nida.nih.gov.

Materials availability—This study did not generate new unique reagents.

Data and code availability—All original code has been deposited at GitHub and is publicly available. The link and DOI listed in the key resource table. All data reported in this paper will be shared by the lead contact upon request. Any additional information required to reanalyze the data reported in this paper is available from the lead contact upon request.

EXPERIMENTAL MODEL AND STUDY PARTICIPANT DETAILS

Subjects—Animals were housed in temperature- and humidity-controlled facilities under a 12 h light/dark cycle with dawn at 0700 h and *ad libitum* chow and water prior to the start of experimental procedures. Mice of both sexes were 2–3 months of age at the start of the experiment (20–40 grams). Strain data and RRIDs are available in the key resource table. Male Sprague Dawley Rats (12–18 weeks; 300–500 grams) were used for tracing experiments and housed in a separate colony under identical conditions. Experiments were conducted in accordance with the USPHP *Guide for the Care and Use of Laboratory Animals* and approved by the Animal Care and Use Committee of the National Institute on Drug Abuse Intramural Research Program.

METHOD DETAILS

Retrograde tracer injection and tissue preparation—Male Sprague Dawley Rats (12–18 weeks; 300–500 grams) were anesthetized with 2–5 % isoflurane (Butler Schein). A 1% Fluorogold (FG; FluoroChrome LLC, RRID AB_2314408) solution in a 0.1M cacodylate buffer (pH 7.5) was delivered unilaterally into the Ventral Tegmental Area (VTA; −3.3mm anteroposterior (AP), −1.0 mm mediolateral (ML), and −4.2 mm dorsoventral (DV)) iontophoretically through a stereotaxically positioned glass micropipette (25–40 μm inner diameter) by applying 2μA pulses in 5s pulses at 10s intervals for 20 min. The micropipette was then left in place for an additional 10 min to prevent backflow. Following surgery, rats were single-housed on a reversed 12 h: 12 h light/dark cycle and perfused 1–3 weeks later. For perfusions Rats were anesthetized with chloral hydrate (0.5 ml/kg) and perfused transcardially with 4% (w/v) paraformaldehyde (PF) in 0.1M phosphate buffer (PB) treated with di-ethylpyrocarbonate (DEPC), pH 7.3. Brains were post-fixed in 4% PF for 2 h before being transferred to an 18% sucrose solution (w/v in 0.1M PB) and stored overnight at 4°C. Coronal sections of the VTA (30 μm) and LPO (16 μm) were prepared.

Localization of retrogradely labeled cells—Sections in the LPO were incubated 24 h at 4°C in primary antibodies (rabbit anti-FG antibody (1:500; AB153; Millipore, RRID AB_2314412), mouse anti-TH antibody (1:200; MAB318, Millipore), goat anti-Calbindin antibody (1:400; ab156812, Abcam), guinea pig anti-Substance-P antibody (1:200; P14103, Neuromics). Sections were then incubated for 2h in corresponding secondary antibodies (647 Alexa Fluor anti-mouse (1:200; 71560517; lot 119241), 594 Alexa Fluor anti-guinea pig (1:200; 706585148; lot 127241), 488 Alexa Fluor anti-rabbit (1:200; 711545152; lot 120705), 405 Dylight anti-goat (1:200, 705475147; lot 117201).

Immunocytochemistry and *in situ* hybridization—Sections in the LPO were incubated for 2 h at 30°C with rabbit anti-FG antibody (1:500; AB153; Millipore, RRID

AB_2314412) supplemented with RNAsin. Testing of the antibody on sections without FG injections or where the primary antibody was omitted did not result in labeling. Sections were then incubated in biotinylated goat anti-rabbit antibody (1:200; BA1000; Vector Laboratories, Burlingame, CA, RRID AB_2313606) for 1 h at 30 °C. Sections were then rinsed and treated with 0.2N HCl, rinsed, and then acetylated in 0.25% acetic anhydride in 0.1M triethanolamine. Subsequently, sections were rinsed and post-fixed with 4% PF, rinsed, and then incubated in a hybridization buffer for 2h at 55° C. Hybridization was then performed either by *in situ* hybridization for radioactive detection of VGaT or VGluT2 mRNA, as previously detailed (Yamaguchi et al., 2007; Yamaguchi et al., 2011).Briefly, sections were hybridized for 16 h at 55 °C with [35S]- and [33P]-labeled (107 c.p.m./ml) single-stranded antisense probes for VGaT (mouse vGaT probe: nucleotides 1–2,814; GenBank accession code: BC052020)or VGluT2 (nucleotides 317–2357; GenBank accession code NM_053427). Following hybridization, sections were treated with 4ug/ml of RNAse A at 37°C for 1 h, washed with 1X saline-sodium citrate and 50% formamide for 1h at 55°C, and then with 0.1X saline-sodium citrate at 68°C for 1h. Subsequently, sections were rinsed with PB and incubated for 1 h at RT in avidin-biotinylated horseradish peroxidase (1:100, ABC kit; Vector Laboratories, RRID AB_2336827). Sections were then rinsed, and the peroxidase reaction was developed with 0.05% 3,3'-diaminobenzidine tetrahydrochloride (DAB) and 0.003% H202. Sections were then photographed under bright field illumination and mounted on coated slides. Finally, slides were dipped in Ilford K.5 nuclear tract emulsion (Polysciences; 1:1 dilution in double-distilled water) and exposed in the dark at 4° C for 3–4 weeks before development and photographs of silver-grain epiluminescence.

Data analysis of *in situ* hybridization studies—Methods for analysis of *in situ* hybridization material have been described previously (Root et al., 2014b). Briefly, pictures were adjusted to match contrast and brightness by using Adobe Photoshop (Adobe Systems). Cell counting was completed blind of injection site by three scorers, and the inter-rater reliability was 94.7%. Radioactive *in situ* material was analyzed using epiluminescence to increase the contrast of silver grains, as described previously (Yamaguchi et al., 2011). Fluorogold positive cells (detected by fluorescence and brown DAB-label) were analyzed to detect the presence of VGaT or VGluT2 mRNA. A cell was considered to express either VGaT or VGluT2 mRNA when its soma contained concentric aggregates of silver grains that exceeded background levels.

Fiber photometry surgeries—Mice were anesthetized with isoflurane (1–4% induction;1% maintenance) and secured to a stereotaxic frame. After exposing the top of the skull, the mouse's head was leveled to ensure the dorsoventral distances between bregma and lambda were within 100 μm of one another. Viruses were injected into the VTA (0.3 μl; AP: −3.2 to −3.4, ML: ± 0.0 to 0.3, DV: −4.3 to −4.4). Injections were made using a Micro4 controller and UltraMicroPump along with 10 μl Nanofil syringes equipped with 35-gauge needles (WPI Inc., Sarasota, FL). Syringes were left in place for 7–10 min following injections to minimize diffusion. For fiber photometry calcium imaging experiments, a 400 μm core optic fiber (Doric Lenses) embedded in a 2.5 mm ferrule was implanted over the LPO (AP: +0.4 to +0.5, ML: ± 0.8 to 0.3, DV: −5.1) and secured to the skull using

#000 screws (Fasteners and Metal products Corp; # 000–120 X 1/16) and dental cement. Following surgery, mice recovered on a warm heating pad before being transferred back to the vivarium home cage. Mice remained in the colony to allow for recovery and virus expression for 3–5 weeks prior to the start of behavioral testing.

Sciatic nerve injections—Similar to methods described previously (Iyer et al., 2014), mice were anesthetized with isoflurane (1–4% induction;1% maintenance) and secured to a stereotaxic frame. Surgical sites were sterilized over the scalp and right flank and the 0.4ml of the local anesthetic 0.25% bupivacaine was injected subcutaneously. A superficial incision was made over the right sciatic nerve. The sciatic nerve was then exposed by blunt dissecting the connective tissue between the gluteus superficialis and biceps femoris. A beveled 35G needle attached by Tygon tubing (0.25mm ID) to a 10ul syringe (World precision instruments) was then inserted under the epineurium of the nerve, taking care to minimize nerve manipulation. 1–2μl of AAV6-hSyn-ChR2-eYFP was then injected into the sciatic nerve at a rate of 1μl/minute. The incision was then closed with absorbable sutures (Vicryl) and VetBond (3M). Following surgery, mice recovered on a warm heating pad before being transferred back to the vivarium home cage. Mice remained in the colony to allow for recovery and virus expression for 3 weeks prior to the start of behavioral testing

Fiber photometry recordings and data analysis—For all recordings, GCaMP6 was excited at two wavelengths (490nm, calcium-dependent signal and 405 nm isosbestic control; Lerner et al., 2015) by amplitude modulated signals from two light-emitting diodes reflected off dichroic mirrors and coupled into a 400μm 0.48NA optic fiber. Signals emitted from GCaMP6s and its isosbestic control channel then returned through the same optic fiber and were acquired using a femtowatt photoreceiver (Model 2151; Newport), digitized at 1kHz, and then recorded by a real-time signal processor (RZ5D; Tucker Davis Technologies) running the Synapse software suite. Analysis of the resulting signal was then performed using custom-written MATLAB scripts. Changes in fluorescence across the experimental session (ΔF/F) were calculated by smoothing signals from the isosbestic control channel (Lerner et al., 2015), scaling the isosbestic control signal by regressing it on the smoothed GCaMP signal, and then generating a predicted 405nm signal using the linear model generated during the regression. Calcium independent signals on the predicted 405nm channel were then subtracted from the raw GCAMP signal to remove movement, photo-bleaching, and fiber bending artifacts. Signals from the GCaMP channel were then divided by the control signal to generate the ΔF/F. Peri-event histograms were then created by averaging changes in fluorescence (ΔF/F) across repeated trials during windows encompassing behavioral events of interest. Video recordings synchronized with neuronal acquisition clocks were ac quired at 30 Hz (RV2, TDT).

Paw withdrawal task and Von Frey apparatus—For our paw withdrawal task, animals were placed on a mesh stand (IITC Life Sciences) inside an 8-inch-tall cylindrical Plexiglas tube. Animals were first injected with 0.9% saline at a volume of 0.01ml per gram of bodyweight. After 15 minutes, animals were then placed inside of the plexiglass cylinder and were given 5 minutes to habituate to their surroundings. Following habituation, the paw ipsilateral to sciatic nerve injections of AAV6-Syn-ChR2-eYFP was stimulated 10

times over the course of 10 minutes using a 473 nm (~10–12 mW) laser. Laser stimulation ended when either the animal withdrew its paw or 10 seconds elapsed; whichever occurred first. Animals were removed from the apparatus and returned to their home cage outside of the experiment room. The procedure was then repeated on subsequent sessions following injections of 5 mg/kg of morphine. For all sessions, fiber photometry recordings were taken and a TTL signal was used to time lock the onset and offset of hindpaw stimulation with the recorded signals.

Pain conditioning task and apparatus—Following post-operative recovery, animals were trained in a pain conditioning paradigm. Animals were placed in a box with a blue LED (470 nm at ~10–12mW) floor (Amuza Inc.). The box was enclosed in a sound attenuating chamber (MED Associates Inc.). Prior to pain conditioning, animals were placed in the LED apparatus for 15 minutes to habituate. After habituation, animals were returned to their home cage for 24 hours. During the following session, animals were placed inside the LED apparatus and given 5 minutes to re-habituate to their surroundings. After habituation, the pain conditioning task was automatically initiated via MEDPC. In this task, a 5 s tone (10,000 Hz @ ~75 dB) predicted the delivery of a 10s blue LED floor stimulation. Stimulations were presented pseudo-randomly 10 times with an average intertrial interval of 60 seconds. Following stimulation, animals were returned to their home cage for 24 hours. This task was repeated three times over three consecutive sessions. We defined these sessions as “Day 1”, “Day 2” and “Day 3”. After Day 3, animals were again returned to their home cage for 24 hours. Finally, animals were placed inside of the LED apparatus. After 5 minutes of habituation, MEDPC automatically initiated a “Cue Test” task. During the Cue Test, the 5 s tone (10,000 Hz @ ~75 dB) was presented 10 times without activation of the LED floor stimulation. As before, the tone was presented pseudo-randomly with an average intertrial interval of 60 s. Throughout the LED floor stimulations, calcium transients were recorded via fiber photometry for the LPO to VTA pathway. For each mouse, the average AUC was calculated for Day 1, Day 2, Day 3 and the Cue Test.

Optogenetics surgeries—Male and female VGluT2::Cre mice (6–12 weeks; 20–35 g; Borgius et al., 2010) or VGaT::Cre mice (Slc32a1tm2(Cre)Lowl/J, in a C57BL/6J background from The Jackson Laboratories, RRID IMSR_JAX:016962) were anesthetized with 1–5% isoflurane and 0.1–0.2 μl AAV5-EF1αa-DIO-ChR2-eYFP (VGluT2-LPO$^{ChR2\text{-}eYFP}$ or VGaT-LPO$^{ChR2\text{-}eYFP}$ mice; experimental group) or AAV5-EF1α-DIO-eYFP (VGluT2-LPO^{eYFP} or VGaT-LPO^{eYFP} mice; control group) was injected into the LPO. For the VTA caspase cell-type specific ablation experiments, an AAV-FLEX-Casp3 was also injected into the VTA of *vglut2::cre* mice (0.3 μl; AP: −3.2 to −3.4, ML: ± 0.0 to 0.3, DV: −4.3 to −4.4). Injections were made using a Micro4 controller and UltraMicro pump along with 10 μl Nanofil syringes equipped with 35-gauge needles (WPI Inc., Sarasota, FL). Syringes were left in place for 7–10 min following injections to minimize diffusion. Following surgery, Mice were group housed on a 12 h:12 h light: dark cycle with dawn at 0700 h. Six to eight weeks after virus injections, mice were either perfused for microscopy or implanted with an optic fiber for behavioral testing (light cycle). Optic fibers for real-time place conditioning were implanted dorsal to the VTA (−3.3, −1.0

ML, −4.2 DV; 10°). Optic fibers for Ca2+ imaging were implanted dorsal to the VTA (−3.3 AP, −0.3 ML, −4.5 DV; 0°).

Real-time place conditioning—Using the three-chamber place conditioning apparatus, VGluT2-LPO$^{ChR2\text{-}eYFP}$, VGluT2-LPO^{eYFP}, VGaT-LPO$^{ChR2\text{-}eYFP}$ and VGaT-LPO^{eYFP} mice were subsequently tested to determine if photostimulation would produce place conditioning or place aversion. For each session, mice were connected to an optical fiber. Mice were first separately habituated to each of the larger conditioning chambers. Subsequently, mice were allowed to freely explore the entire apparatus to establish baseline responding over a 15-minute test. Mice showing a side preference prior to training were excluded. Over four 30-minute conditioning days, one chamber was assigned as the photostimulation-paired chamber (counterbalanced across all mice). The two different chambers were differentiated by the presence or absence of visually distinct stripes on the walls of the chamber. Mice were given light stimulation through the optic fiber (473nm, ~7mW, 10ms duration, 20 Hz) in the VTA whenever they entered the photostimulation-paired chamber. Mice were then tested for a place preference in the absence of photostimulation for 15-minutes. Following the first stage of conditioning, photostimulation was shifted to the opposite conditioning chamber for four conditioning chambers (Reversal Sessions 1–4; 30-minutes). Upon the completion of reversal training, mice were again tested (15-minutes) in the absence of photostimulation. All experimental procedures were controlled by video tracking software (AnyMaze, Stoelting).

c-Fos immunolabeling and RNAscope—The phenotyping of VTA c-Fos was done by combination of immunodetection of c-Fos (phospho-c-Fos rabbit mAb #5348 at 1:400 dilution, Cell Signaling Technology, Inc., Danvers, MA) and TH (mouse anti-TH antibody at 1:1000 dilution, MAB318, Millipore, Burlington, MA) and detection of transcripts encoding VGluT2 and VGaT mRNA by RNAscope. Midbrain coronal free-floating sections (16 μm) were rinsed with DEPC-treated PB. Sections were incubated with a cocktail of anti c-Fos and anti TH antibodies for 2 h at 30°C, rinsed and incubated with secondary donkey anti-rabbit Alexa Fluor 647 (1:100, 711–605-152, Jackson ImmunoResearch, West Grove, PA) and donkey anti-mouse Alexa Fluor 750 (1:100, ab175738, abcam, Cambridge, MA) for 1 h at 30°C. Sections were rinsed with DEPC-treated PB and then were mounted onto Fisher SuperFrost slides and dried overnight at 60°C. RNAscope *in situ* hybridization was performed according to the manufacturer's instructions. Briefly, sections were treated with heat and protease digestion followed by hybridization with a mixture containing target probes to mouse VGluT2 (319171, Advanced Cell Diagnostics, Newark, CA) and mouse VGaT (319191-C3, Advanced Cell Diagnostics, Newark, CA). Additional sections were hybridized with the bacterial gene DapB as a negative control, which did not exhibit fluorescent labeling. VGluT2 and VGaT were detected by Atto 550 and Alexa 488. RNAscope *in situ* hybridization and immunolabeled sections were viewed, analyzed, and photographed with a Zeiss LSM880 confocal microscope. Negative control hybridizations showed negligible fluorophore expression. Neurons were counted when the stained cell was at least 5 μm in diameter. Pictures were adjusted to match contrast and brightness by using Adobe Photoshop (Adobe Systems). The number of mice (n = 3/group; 15 sections/mouse)

analyzed was based on previous studies in our lab using radioactive detection of VGluT2 mRNA from rat VTA neurons (Yamaguchi et al., 2011).

Confocal fluorescence microscopy—Free floating coronal sections (40 μm) from *vglut2:cre* mice with viral injection of AAV5-CaMKII-ChR2-mCherry into the LPO and AAV5-DIO-ChR2-eYFP into the VTA (n = 3) and VGaT::Cre mice with viral injection of AAV5-CaMKII-ChR2-mCherry into the LPO and AAV5-DIO-ChR2-eYFP into the VTA (n = 3) were incubated for 1 h in PB supplemented with 4% BSA and 0.3% Triton X-100. Sections were then incubated with cocktails of primary antibodies: mouse anti-mCherry (1:500, Takara, #632543) + goat anti-VGluT2 (1:500, Frontier Institute, VGluT2-Go-Af310) + Guinea pig anti-VGaT (1:500, Frontier Institute, VGAT-GP-Af1000) + rabbit anti-TH (1:1000, Millipore Sigma, AB152), overnight at 4°C. After rinsing 3 × 10 min in PB, sections were incubated in a cocktail of the corresponding fluorescence secondary antibodies: DyLight-405-donkey anti-guinea pig (706475148; Jackson ImmunoResearch Laboratories) + Alexa-Fluor-594-donkey anti-mouse (715585151, Jackson ImmunoResearch Laboratories) + Alexa-Fluor-647-donkey anti-goat (705605147, Jackson ImmunoResearch Laboratories) + Alexa-Fluor-750-donkey anti-rabbit (ab175731, abcam) for 2 h at room temperature. After rinsing, sections were mounted on slides. Fluorescent images were collected with a Zeiss LSM880 with Cy7.5 Confocal System (Zeiss). Images were taken sequentially with different lasers with 20× and 63× oil immersion objectives and Z-axis stacks were collected at 0.2 μm. This experiment was successfully repeated three times.

Electron microscopy—Vibratome tissue sections (40 μm) from *vglut2:cre* mice with viral injection of AAV5-CaMKII-ChR2-mCherry into the LPO and AAV5-DIO-ChR2-eYFP into the VTA (n = 3) and VGaT::Cre mice with viral injection of AAV5-CaMKII-ChR2-mCherry into the LPO and AAV5-DIO-ChR2-eYFP into the VTA (n = 3) were rinsed and incubated with 1% sodium borohydride to inactivate free aldehyde groups, rinsed, and then incubated with blocking solution. Sections were then incubated with primary antibodies [mouse anti-mCherry (1:1,000), guinea pig anti-VGluT2 (1:500, Frontier Institute, VGluT2-GP-Af810) and rabbit anti-GFP (1:2000, Frontier Institute, GFP-Rb-Af2020)]; or primary antibodies [mouse anti-mCherry (1:1,000), guinea pig anti-VGaT (1:500) and rabbit anti-GFP (1:2000)]; or primary antibodies [mouse anti-mCherry (1:1,000), guinea pig anti-VGluT2 (1:500) and rabbit anti-TH (1:1000)]; or primary antibodies [mouse anti-mCherry (1:1,000), guinea pig anti-VGaT (1:500) and rabbit anti-TH (1:1000)]. All primary antibodies were diluted with 1% normal goat serum (NGS), 4% BSA in PB supplemented with 0.02% saponin and incubations were for 24 h at 4°C. Sections were rinsed and incubated overnight at 4°C in the corresponding secondary antibodies. Sections were rinsed in PB, and then in double-distilled water, followed by silver enhancement of the gold particles with the Nanoprobe Silver Kit (2012, Nanoprobes) for 7 min at room temperature. Next, sections were incubated in avidin-biotinylated horseradish peroxidase complex in PB for 2 h at room temperature and washed. Peroxidase activity was detected with 0.025% 3,3'-diaminobenzidine (DAB) and 0.003% H_2O_2 in PB for 5–10 min. Sections were rinsed with PB and fixed with 0.5% osmium tetroxide in PB for 25 min, washed in PB, followed by double distilled water, and then contrasted in freshly prepared 1% uranyl acetate for 35 min. Sections were dehydrated through a series of graded alcohols

and with propylene oxide. Afterwards, they were flat embedded in Durcupan ACM epoxy resin (14040, Electron Microscopy Sciences). Resin-embedded sections were polymerized at 60°C for 2 days. Sections of 60 nm were cut from the outer surface of the tissue with an ultramicrotome UC7 (Leica Microsystems) using a diamond knife (Diatome). The sections were collected on formvar-coated single slot grids and counterstained with Reynolds lead citrate. Sections were examined and photographed using a Tecnai G_2 12 transmission electron microscope (Fei Company) equipped with the OneView digital micrograph camera (Gatan). Ultrastructural analysis. Serial ultrathin sections of the VTA (bregma −2.92 mm to −3.80 mm) from were analyzed. Synaptic contacts were classified according to their morphology and immunolabel and photographed at a magnification of 6,800–13,000×. The morphological criteria used for identification and classification of cellular components or type of synapse observed in these thin sections were as previously described (Zhang et al, 2015). In the serial sections, a terminal containing greater than 5 immunogold particles was considered as immunopositive terminal. Pictures were adjusted to match contrast and brightness by using Adobe Photoshop (Adobe Systems Incorporated, Seattle, WA). This experiment was successfully repeated three times. Electron microscopy and confocal analysis quantification were blinded.

***Ex vivo* electrophysiology—**Eight weeks after virus injection, VGluT2::Cre, TH::Cre or VGaT::Cre mice carrying AAV5-CaMKII-ChR2-mCherry in the LPO and AAV1-DIO-eYFP in the VTA were anesthetized with isoflurane, decapitated and the Brain was quickly removed and placed in ice-cold artificial cerebrospinal fluid (ACSF), saturated with 95% O_2 and 5% CO_2, and modified to contain (in mM): 92 NMDG, 20 HEPES, 25 glucose, 30 $NaHCO_3$, 1.2 NaH_2PO_4, 2.5 KCl, 5 sodium ascorbate, 3 sodium pyruvate, 2 thiourea, 10 $MgSO_4$, 0.5 $CaCl_2$. VTA horizontal slices of 200 μm thickness were obtained using a VT-1200 vibratome (Leica, Nussloch, Germany) and then placed in a holding chamber filled with the same solution, but held at 32°C. After 15 min, slices were transferred to a holding chamber containing room temperature aCSF modified to contain (in mM): 92 NaCl, 20 HEPES, 25 glucose, 30 $NaHCO_3$, 1.2 NaH_2PO_4, 2.5 KCl, 5 sodium ascorbate, 3 sodium pyruvate, 2 thiourea, 1 $MgSO_4$, 2 $CaCl_2$. For recordings, slices were transferred to a chamber perfused with 32°C aCSF modified to contain (in mM): 125 NaCl, 2.5 KCl, 1.25 NaH_2PO_4, 1 $MgCl_2$, 2.4 $CaCl_2$, 26 $NaHCO_3$ and 11 glucose. Electrodes (3–6MΩ) were backfilled with a potassium gluconate internal solution containing (in mM): 140 potassium gluconate, 2 NaCl, 1.5 $MgCl_2$, 10 HEPES, 4 Mg-ATP, 0.3 Na2-GTP, 10 Naphosphocreatine, 0.1 EGTA and 0.2% biocytin (pH 7.2; 280–290 mOsm), for current clamp recordings or with a Cesium methansulfonate internal solution containing (in mM): 124 CsMeSO4, 11 KCl, 0.1 EGTA, 10 HEPES, 10 Na_2 Phosphocreatine, 4 Mg-ATP, 0.3 Na_2-GTP, 0.5 % Biocytin (pH 7.2; 280 mOsm), for voltage clamp recordings.. Cells were visualized on an upright microscope using infrared differential interference contrast video microscopy. Whole-cell voltage-clamp or current clamp recordings were made using a MultiClamp 700B amplifier (2 kHz low-pass Bessel filter and 10 kHz digitization) with pClamp 10.3 software (Molecular Devices, Sunnyvale, CA). VTA VGluT2, TH or VGaT neurons were identified by expression of eYFP. Neurons were voltage clamped at −60 mV or 0 mV. Series resistance (10–30 MΩ) was monitored with a 5mV hyperpolarizing pulse (50 ms) given every 10 s, and only recordings that remained stable over the period of data collection were used. A 200

μm core optical fiber, coupled to a diode-pumped solid-state laser, was positioned just above the slice, and aimed at the recorded cell. Optically-evoked EPSCs or IPSCs were obtained every 10 s with pulses of 473 nm wavelength light (8 mW, 5–10 ms). After evoking EPSCs or IPSCs, the peak amplitude was measured with the average of 20 consecutive traces. In a subset of recordings used to determine the monosynaptic nature of LPO→LHb EPSCs, TTX (1 μM), followed by TTX + 4-AP (200 μM), and finally the addition of CNQX (10 μM) were bath applied.

Chemogenetic surgeries—Mice were anesthetized with isoflurane (1–4% induction; 1% maintenance) and secured to a stereotaxic frame. After exposing the top of the skull, the mouse's head was leveled to ensure the dorsoventral distances between bregma and lambda were within 100 μm of one another. A retrograde virus encoding the cre-dependent inhibitory DREADD, HSV-LSIL-hM4Di-mCherry were injected into the VTA (0.3 μl; AP: −3.2 to −3.4, ML: ± 0.0 to 0.3, DV: −4.3 to −4.4). Injections were made using a Micro4 controller and UltraMicroPump along with 10 μl Nanofil syringes equipped with 35-gauge needles (WPI Inc., Sarasota, FL). Syringes were left in place for 7–10 min following injections to minimize diffusion. For circuit-specific chemogenetic inhibition, a cannular (Plastics One) was implanted over the LPO (AP: +0.4 to +0.5, ML: ± 0.8 to 0.3, DV: −5.1) and secured to the skull using #000 screws (Fasteners and Metal products Corp; # 000–120 X 1/16) and dental cement. Following surgery, mice recovered on a warm heating pad before being transferred back to the vivarium home cage. Mice remained in the colony to allow for recovery and virus expression for 3–5 weeks prior to the start of behavioral testing.
Formalin Footpad Test. Mice were given an injection of JHU 37160 ("J60"; 200 nl, 0.1 ug/ul, in acsf) or acsf (200nl) 15 minutes prior to testing. The hindpaw of mice was then injected with a 1% solution of formalin (20μl). Mice were then placed in a clear cylindrical container with a 4" diameter for 1 hour. Nocifensive licking responses were quantified across the entire session and broken into two phases: 1) Phase I was defined as 0–5 minutes of the session 2) Phase II was defined as the period between 20–60 minutes.

Sucrose licking task—Mice were restricted to 85% free-feeding body weight for the duration of the sucrose reward test. Two days prior to training, mice were pre-exposed to 8% sucrose in their home cage for 1 hour. One day prior to training, mice were habituated to the operant chamber for 30 min. On days 1–4 of training, mice were placed in an operant chamber containing one bottle of 8% sucrose for 1 hour (one session /per day). Licking responses for the sucrose bottle were recorded by a contact Lickometer (ENV-250, Med Associates) throughout the session and bottled were weighed before and after each session. On day 5, intra-LPO administration of artificial cerebrospinal fluid (acsf, 200 nl) or JHU 37160 ("J60"; 200 nl, 0.1 ug/ul, in acsf) was given 15 min before mice were placed in the operant chamber. Responding on day 4 was used as a pre-treatment baseline and compared to responses on day 5.

QUANTIFICATION AND STATISTICAL ANALYSIS

Statistics

ANOVAs were used to compare effects, except when the data were non-normally distributed. The sphericity assumption for repeated measures ANOVAs was assessed with the Mauchly sphericity test; when the outcome was significant the F values were corrected using the Greenhouse-Geisser approach. Data with a non-normal distribution were examined using a Generalized Linear Model (GLM). For between-subjects comparisons, a Tukey post-hoc correction was used, while a Sidak-holm or Neman-Keuls correction was applied for all other analyses. Statistical analyses were performed with SPSS or Prism. Alpha was always set at $p < 0.05$.

Sample size

The target number of samples in each group for behavioral, anatomical, and electrophysiological experiments was determined on the basis of sufficiently powered experiments reported in published studies. The experimenter performing surgeries, including virus vector injection and probe or cannula implantation, was known to hit the targets used (LPO or LHb) with a probability of 0.9. Our target number of animals in each group was ten. We therefore performed about 12 surgeries in each group. The numbers of subjects for each experiment can be found in the main text and figure captions.

Randomization

All randomization was performed by an experimenter. The same stereotaxic apparatus was used for all surgeries. All surgical and behavioral manipulations performed on each animal were determined randomly. For animals used in behavioral experiments, the virus used in each animal and injection site were determined randomly and counterbalanced across groups.

Exclusion criteria

Data were excluded on the basis of predetermined histological and performance criteria established during pilot experiments. Histological criteria included injection sites and optical fiber or guide cannula placement. Only animals with injection sites in the region of interest were included.

Supplementary Material

Refer to Web version on PubMed Central for supplementary material.

ACKNOWLEDGMENTS

We are grateful for the assistance of Rong Ye, Kevin Yu, and Dylan Sucich with electron microscopy experiments; Robert Juza with the optogenetics experiments; and Orlando Espinoza and Uzma Mohammad with formalin footpad test experiments. This work was supported by the Intramural Research Program of the National Institute on Drug Abuse, US National Institutes of Health (IRP/NIDA/NIH), and a K99/R00 Pathway to Independence award from the National Institute on Drug Abuse, DA043572 (D.J.B.).

INCLUSION AND DIVERSITY

One or more of the authors of this paper self-identifies as an underrepresented ethnic minority in their field of research or within their geographical location. One or more of the authors of this paper self-identifies as a gender minority in their field of research. We support inclusive, diverse, and equitable conduct of research.

REFERENCES

1. Fishbain DA, Cutler R, Rosomoff HL, and Rosomoff RS (1997). Chronic pain-associated depression: antecedent or consequence of chronic pain? A review. Clin. J. Pain 13, 116–137. [PubMed: 9186019]
2. Volkow ND, and McLellan AT (2016). Opioid Abuse in Chronic Pain–Misconceptions and Mitigation Strategies. N. Engl. J. Med. 374, 1253–1263. [PubMed: 27028915]
3. Berna C, Leknes S, Holmes EA, Edwards RR, Goodwin GM, and Tracey I (2010). Induction of depressed mood disrupts emotion regulation neurocircuitry and enhances pain unpleasantness. Biol. Psychiatr. 67, 1083–1090.
4. Garland EL, Froeliger B, Zeidan F, Partin K, and Howard MO (2013). The downward spiral of chronic pain, prescription opioid misuse, and addiction: cognitive, affective, and neuropsychopharmacologic pathways. Neurosci. Biobehav. Rev 37 (10 Pt 2), 2597–2607. [PubMed: 23988582]
5. de Wied M, and Verbaten MN (2001). Affective pictures processing, attention, and pain tolerance. Pain 90, 163–172. [PubMed: 11166983]
6. Kirwilliam SS, and Derbyshire SWG (2008). Increased bias to report heat or pain following emotional priming of pain-related fear. Pain 137, 60–65. [PubMed: 17881129]
7. Linton SJ, and Bergbom S (2011). Understanding the link between depression and pain. Scand. J. Pain 2, 47–54. [PubMed: 29913734]
8. Wade JB, Price DD, Hamer RM, Schwartz SM, and Hart RP (1990). An emotional component analysis of chronic pain. Pain 40, 303–310. [PubMed: 2326095]
9. de Heer EW, Gerrits MMJG, Beekman ATF, Dekker J, van Marwijk HWJ, de Waal MWM, Spinhoven P, Penninx BWJH, and van der Feltz-Cornelis CM (2014). The association of depression and anxiety with pain: a study from NESDA. PLoS One 9, e106907. [PubMed: 25330004]
10. Fields HL, and Margolis EB (2015). Understanding opioid reward. Trends Neurosci. 38, 217–225. [PubMed: 25637939]
11. Scardochio T, Trujillo-Pisanty I, Conover K, Shizgal P, and Clarke PBS (2015). The Effects of Electrical and Optical Stimulation of Midbrain Dopaminergic Neurons on Rat 50-kHz Ultrasonic Vocalizations. Front. Behav. Neurosci. 9, 331. [PubMed: 26696851]
12. Groppe SE, Gossen A, Rademacher L, Hahn A, Westphal L, Gründer G, and Spreckelmeyer KN (2013). Oxytocin influences processing of socially relevant cues in the ventral tegmental area of the human brain. Biol. Psychiatr. 74, 172–179.
13. Friedman A, Frankel M, Flaumenhaft Y, Merenlender A, Pinhasov A, Feder Y, Taler M, Gil-Ad I, Abeles M, and Yadid G (2009). Programmed acute electrical stimulation of ventral tegmental area alleviates depressive-like behavior. Neuropsychopharmacology 34, 1057–1066. [PubMed: 18843267]
14. Shumake J, and Gonzalez-Lima F (2003). Brain systems underlying susceptibility to helplessness and depression. Behav. Cognit. Neurosci. Rev. 2, 198–221. [PubMed: 15006293]
15. Morales M, and Margolis EB (2017). Ventral tegmental area: cellular heterogeneity, connectivity and behaviour. Nat. Rev. Neurosci. 18, 73–85. [PubMed: 28053327]
16. Barker DJ, Root DH, Zhang S, and Morales M (2016). Multiplexed neurochemical signaling by neurons of the ventral tegmental area. J. Chem. Neuroanat. 73, 33–42. [PubMed: 26763116]
17. Taylor AMW, Becker S, Schweinhardt P, and Cahill C (2016). Mesolimbic dopamine signaling in acute and chronic pain: implications for motivation, analgesia, and addiction. Pain 157, 1194–1198. [PubMed: 26797678]

18. Morgan MJ, and Franklin KB (1990). 6-Hydroxydopamine lesions of the ventral tegmentum abolishd-amphetamine and morphine analgesia in the formalin test but not in the tail flick test. Brain Res. 519, 144–149. [PubMed: 2118819]
19. Saadé NE, Atweh SF, Bahuth NB, and Jabbur SJ (1997). Augmentation of nociceptive reflexes and chronic deafferentation pain by chemical lesions of either dopaminergic terminals or midbrain dopaminergic neurons. Brain Res. 751, 1–12. [PubMed: 9098562]
20. Navratilova E, Xie JY, Okun A, Qu C, Eyde N, Ci S, Ossipov MH, King T, Fields HL, and Porreca F (2012). Pain relief produces negative reinforcement through activation of mesolimbic reward-valuation circuitry. Proc. Natl. Acad. Sci. USA 109, 20709–20713. [PubMed: 23184995]
21. Niikura K, Narita M, Narita M, Nakamura A, Okutsu D, Ozeki A, Kurahashi K, Kobayashi Y, Suzuki M, and Suzuki T (2008). Direct evidence for the involvement of endogenous beta-endorphin in the suppression of the morphine-induced rewarding effect under a neuropathic pain-like state. Neurosci. Lett. 435, 257–262. [PubMed: 18359165]
22. Hipólito L, Wilson-Poe A, Campos-Jurado Y, Zhong E, Gonzalez-Romero J, Virag L, Whittington R, Comer SD, Carlton SM, Walker BM, et al. (2015). Inflammatory Pain Promotes Increased Opioid Self-Administration: Role of Dysregulated Ventral Tegmental Area mu Opioid Receptors. J. Neurosci. 35, 12217–12231. [PubMed: 26338332]
23. Ko MY, Jang EY, Lee JY, Kim SP, Whang SH, Lee BH, Kim HY, Yang CH, Cho HJ, and Gwak YS (2018). The Role of Ventral Tegmental Area Gamma-Aminobutyric Acid in Chronic Neuropathic Pain after Spinal Cord Injury in Rats. J. Neurotrauma 35, 1755–1764. [PubMed: 29466910]
24. Yetnikoff L, Cheng AY, Lavezzi HN, Parsley KP, and Zahm DS (2015). Sources of input to the rostromedial tegmental nucleus, ventral tegmental area, and lateral habenula compared: A study in rat. J. Comp. Neurol. 523, 2426–2456. [PubMed: 25940654]
25. Burstein R, Cliffer KD, and Giesler GJ Jr. (1987). Direct somatosensory projections from the spinal cord to the hypothalamus and telencephalon. J. Neurosci. 7, 4159–4164. [PubMed: 3694268]
26. Burstein R, Cliffer KD, and Giesler GJ Jr. (1990). Cells of origin of the spinohypothalamic tract in the rat. J. Comp. Neurol. 291, 329–344. [PubMed: 2298937]
27. Burstein R, Falkowsky O, Borsook D, and Strassman A (1996). Distinct lateral and medial projections of the spinohypothalamic tract of the rat. J. Comp. Neurol. 373, 549–574. [PubMed: 8889944]
28. Cliffer KD, Burstein R, and Giesler GJ Jr. (1991). Distributions of spinothalamic, spinohypothalamic, and spinotelencephalic fibers revealed by anterograde transport of PHA-L in rats. J. Neurosci. 11, 852–868. [PubMed: 1705972]
29. Li JL, Kaneko T, Shigemoto R, and Mizuno N (1997). Distribution of trigeminohypothalamic and spinohypothalamic tract neurons displaying substance P receptor-like immunoreactivity in the rat. J. Comp. Neurol. 378, 508–521. [PubMed: 9034907]
30. Almli CR, and McMullen NT (1979). Ontogeny of lateral preoptic unit activity in rats. Brain Res. Bull. 4, 773–781. [PubMed: 316722]
31. Ono T, and Nakamura K (1985). Learning and integration of rewarding and aversive stimuli in the rat lateral hypothalamus. Brain Res. 346, 368–373. [PubMed: 4052786]
32. Silva E, Hernandez L, Quiñonez B, Gonzalez LE, and Colasante C (2004). Selective amino acids changes in the medial and lateral preoptic area in the formalin test in rats. Neuroscience 124, 395–404. [PubMed: 14980389]
33. Hori T, Oka T, Hosoi M, and Aou S (1998). Pain modulatory actions of cytokines and prostaglandin E2 in the brain. Ann. N. Y. Acad. Sci. 840, 269–281. [PubMed: 9629255]
34. Geisler S, Derst C, Veh RW, and Zahm DS (2007). Glutamatergic afferents of the ventral tegmental area in the rat. J. Neurosci. 27, 5730–5743. [PubMed: 17522317]
35. Iyer SM, Montgomery KL, Towne C, Lee SY, Ramakrishnan C, Deisseroth K, and Delp SL (2014). Virally mediated optogenetic excitation and inhibition of pain in freely moving nontransgenic mice. Nat. Biotechnol. 32, 274–278. [PubMed: 24531797]
36. Iyer SM, Vesuna S, Ramakrishnan C, Huynh K, Young S, Berndt A, Lee SY, Gorini CJ, Deisseroth K, and Delp SL (2016). Optogenetic and chemogenetic strategies for sustained inhibition of pain. Sci. Rep. 6, 30570. [PubMed: 27484850]

37. Towne C, Montgomery KL, Iyer SM, Deisseroth K, and Delp SL (2013). Optogenetic control of targeted peripheral axons in freely moving animals. PLoS One 8, e72691. [PubMed: 23991144]
38. Yamaguchi T, Qi J, Wang HL, Zhang S, and Morales M (2015). Glutamatergic and dopaminergic neurons in the mouse ventral tegmental area. Eur. J. Neurosci. 41, 760–772. [PubMed: 25572002]
39. Root DH, Wang HL, Liu B, Barker DJ, Mó d L, Szocsics P, Silva AC, Maglóczky Z, and Morales M (2016). Glutamate neurons are intermixed with midbrain dopamine neurons in nonhuman primates and humans. Sci. Rep. 6, 30615. [PubMed: 27477243]
40. Bouarab C, Thompson B, and Polter AM (2019). VTA GABA Neurons at the Interface of Stress and Reward. Front. Neural Circuits 13, 78. [PubMed: 31866835]
41. Root DH, Barker DJ, Estrin DJ, Miranda-Barrientos JA, Liu B, Zhang S, Wang HL, Vautier F, Ramakrishnan C, Kim YS, et al. (2020). Distinct Signaling by Ventral Tegmental Area Glutamate, GABA, and Combinatorial Glutamate-GABA Neurons in Motivated Behavior. Cell Rep. 32, 108094. [PubMed: 32877676]
42. Brischoux F, Chakraborty S, Brierley DI, and Ungless MA (2009). Phasic excitation of dopamine neurons in ventral VTA by noxious stimuli. Proc. Natl. Acad. Sci. USA 106, 4894–4899. [PubMed: 19261850]
43. Verharen JPH, Zhu Y, and Lammel S (2020). Aversion hot spots in the dopamine system. Curr. Opin. Neurobiol. 64, 46–52. [PubMed: 32146296]
44. Root DH, Mejias-Aponte CA, Qi J, and Morales M (2014). Role of glutamatergic projections from ventral tegmental area to lateral habenula in aversive conditioning. J. Neurosci. 34, 13906–13910. [PubMed: 25319687]
45. Qi J, Zhang S, Wang HL, Barker DJ, Miranda-Barrientos J, and Morales M (2016). VTA glutamatergic inputs to nucleus accumbens drive aversion by acting on GABAergic interneurons. Nat. Neurosci. 19, 725–733. [PubMed: 27019014]
46. Wang HL, Qi J, Zhang S, Wang H, and Morales M (2015). Rewarding Effects of Optical Stimulation of Ventral Tegmental Area Glutamatergic Neurons. J. Neurosci. 35, 15948–15954. [PubMed: 26631475]
47. Mileykovskiy B, and Morales M (2011). Duration of inhibition of ventral tegmental area dopamine neurons encodes a level of conditioned fear. J. Neurosci. 31, 7471–7476. [PubMed: 21593330]
48. Taylor NE, Long H, Pei J, Kukutla P, Phero A, Hadaegh F, Abdelnabi A, Solt K, and Brenner GJ (2019). The rostromedial tegmental nucleus: a key modulator of pain and opioid analgesia. Pain 160, 2524–2534. [PubMed: 31246732]
49. Schultz W, and Dickinson A (2000). Neuronal coding of prediction errors. Annu. Rev. Neurosci. 23, 473–500. [PubMed: 10845072]
50. Weiss JM (1970). Somatic effects of predictable and unpredictable shock. Psychosom. Med. 32, 397–408. [PubMed: 5535207]
51. Gliner JA (1972). Predictable vs. unpredictable shock: preference behavior and stomach ulceration. Physiol. Behav. 9, 693–698. [PubMed: 4676259]
52. Abbott BB, Schoen LS, and Badia P (1984). Predictable and unpredictable shock: behavioral measures of aversion and physiological measures of stress. Psychol. Bull. 96, 45–71. [PubMed: 6463164]
53. Lejuez CW, Eifert GH, Zvolensky MJ, and Richards JB (2000). Preference between onset predictable and unpredictable administrations of 20% carbon-dioxide-enriched air: Implications for better understanding the etiology and treatment of panic disorder. J. Exp. Psychol. Appl. 6, 349–358. [PubMed: 11218343]
54. Lockard JS (1963). Choice of a warning signal or no warning signal in an unavoidable shock situation. J. Comp. Physiol. Psychol. 56, 526–530. [PubMed: 13931179]
55. Orsini C, Ventura R, Lucchese F, Puglisi-Allegra S, and Cabib S (2002). Predictable stress promotes place preference and low mesoaccumbens dopamine response. Physiol. Behav. 75, 135–141. [PubMed: 11890962]
56. Guile MN, and McCutcheon NB (1984). Effects of naltrexone and signaling inescapable electric shock on nociception and gastric lesions in rats. Behav. Neurosci. 98, 695–702. [PubMed: 6540590]

57. Dombrowski PA, Maia TV, Boschen SL, Bortolanza M, Wendler E, Schwarting RKW, Brandão ML, Winn P, Blaha CD, and Da Cunha C (2013). Evidence that conditioned avoidance responses are reinforced by positive prediction errors signaled by tonic striatal dopamine. Behav. Brain Res. 241, 112–119. [PubMed: 22771418]

Highlights

- LPO glutamate neurons send information about nociceptive stimuli to the VTA
- LPO→VTA GABA neurons mediate reward and are activated during predictable pain
- LPO glutamate or GABA neurons make strong synapses on VTA GABA neurons
- Inhibiting LPO glutamate neurons mitigates the aversiveness of pain

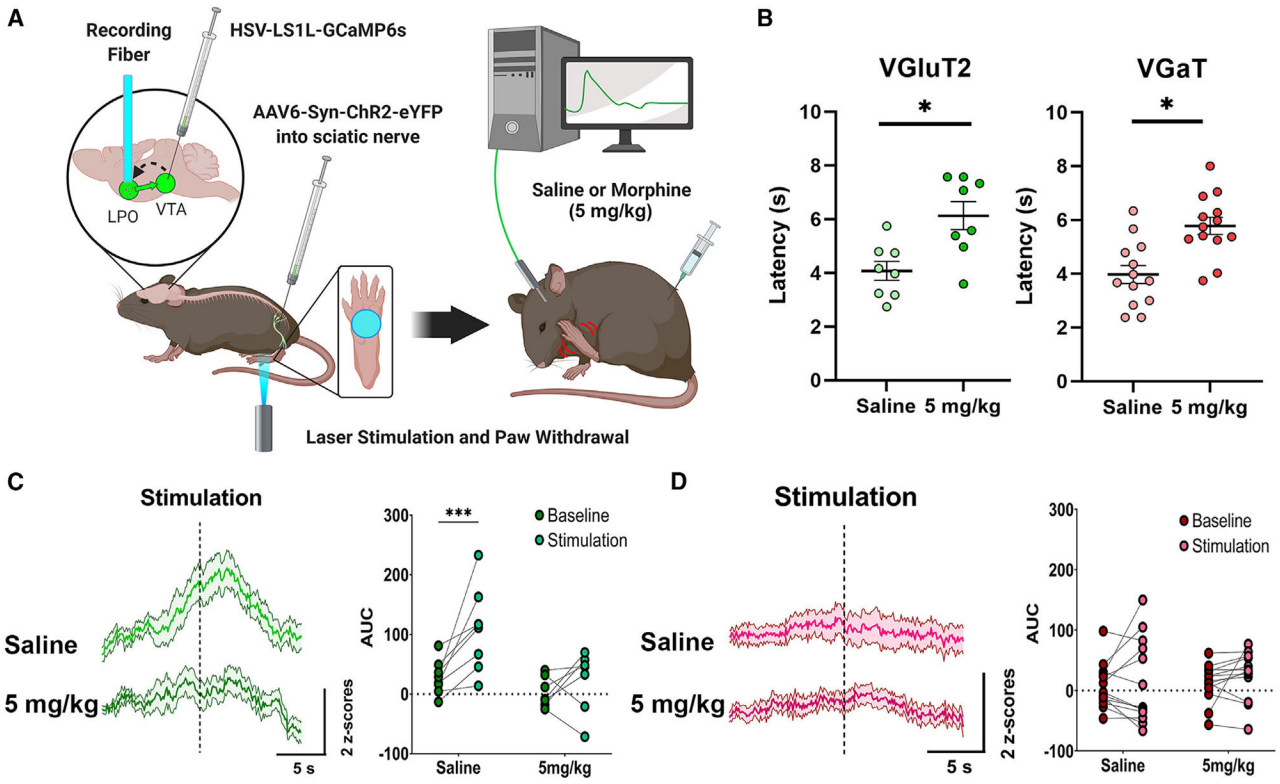

Figure 1. Inputs from LPO VGluT2 neurons to the VTA signal nociceptive stimuli

(A) Diagram of surgical procedures and recording task. Retrograde Cre-dependent HSV-LS1L-GCaMP6s viral vector was injected into the VTA of *vglut2:cre* or *vgat:cre* mice and retrograde AAV6-Syn-ChR2-eYFP viral vector was injected into the sciatic nerve. An optic fiber was implanted over the LPO for fiber photometry calcium imaging recordings of LPO-VGluT2 or LPO-VGaT neurons innervating the VTA in response to laser-induced nocifensive responses after injection of saline or morphine (5 mg/kg).

(B) Latency to paw withdrawal induced by sciatic nerve laser stimulation in *vglut2:cre* or *vgat:cre* mice after injections of saline or morphine (5 mg/kg) (mixed ANOVA; VGluT2 n = 8, $F_{(2,23)} = 8.516$, p = 0.007; VGaT n = 13, $F_{(2,38)} = 6.61$, p = 0.005; *p < 0.05; data represent the mean ± SEM).

(C) LPO-VGluT2 neurons innervating the VTA signal the nociceptive stimulation of the paw, which is blocked by morphine (5 mg/kg) (***p < 0.001).

(D) LPO-VGaT neurons innervating the VTA do not show responses to the nociceptive stimulation of the paw or morphine (mixed ANOVA; $F_{(2,38)} = 3.123$, p = 0.032; data represent the mean ± SEM). (See also Figures S2 and S3.)

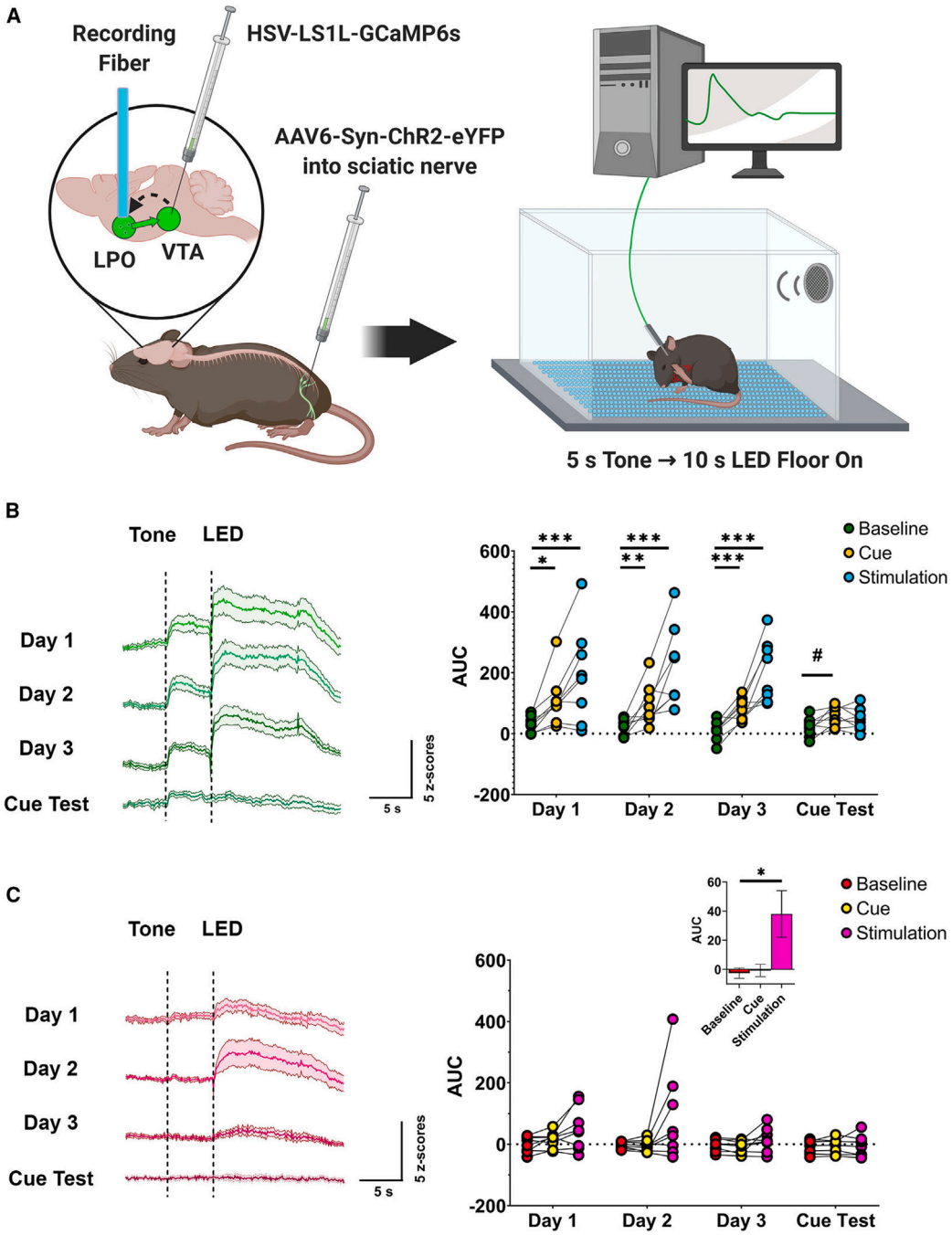

Figure 2. Inputs from LPO VGluT2 neurons to the VTA play a role in cue-induced nociception

(A) Diagram of surgical procedures and recording task. Retrograde Cre-dependent HSV-LS1L-GCaMP6s viral vector was injected into the VTA of *vglut2:cre* or *vgat:cre* mice and the retrograde AAV6-Syn-ChR2-eYFP viral vector was injected into the sciatic nerve. An optic fiber was implanted over the LPO for fiber photometry calcium imaging recordings of LPO-VGluT2 or LPO-VGaT neurons innervating the VTA in response to a pain conditioning task, where a 5 s tone predicted 10 s of nociceptive induced by intra-sciatic stimulation through an LED floor.

(B) LPO-VGluT2 neurons innervating the VTA signal both a cue predicting the onset of stimulation and the delivery of nociceptive stimulation (generalized linear model; n = 8; session × epoch interaction, $\chi^2_{(6)} = 33.58$, $p < 0.0001$; *$p < 0.05$, **$p < 0.01$, ***$p < 0.001$; $^{\#}p = 0.063$; data represent the mean ± SEM).

(C) LPO-VGaT neurons innervating the VTA signal predictable nociceptive stimulation (generalized linear model; n = 8; main effect of epoch [inset], $\chi^2_{(2)} = 7.58$, $p = 0.023$; *$p < 0.05$; data represent the mean ± SEM). (See also Figures S2 and S3.)

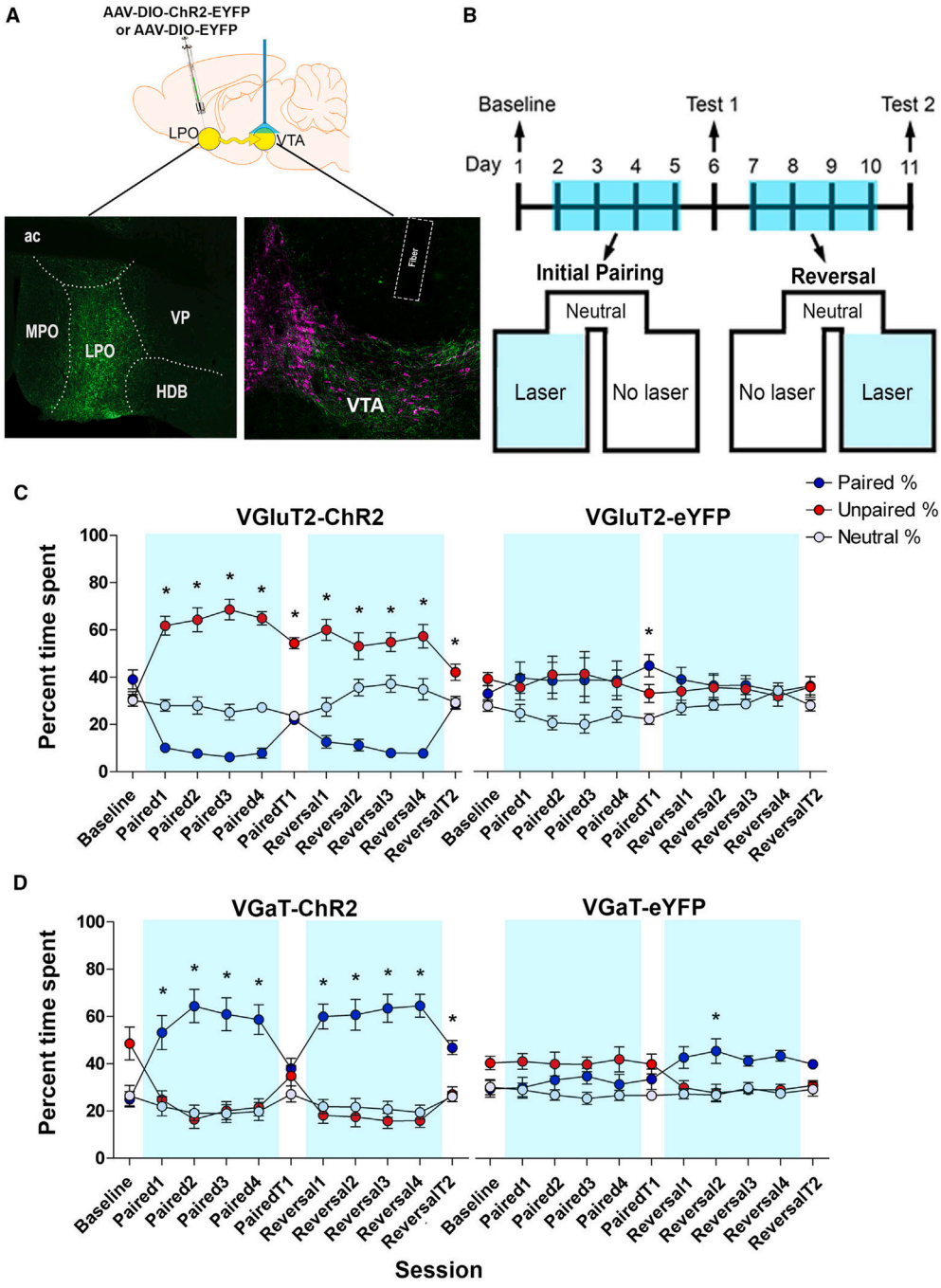

Figure 3. VTA photostimulation of LPO-VGaT fibers is rewarding and VTA photostimulation of LPO-VGluT2 fibers is aversive

(A) Diagram of virus injection (AAV5-EF1αa-DIO-ChR2-eYFP or AAV5-EF1α-DIO-eYFP) into the LPO and VTA photostimulation of LPO-VGluT2 or LPO-VGaT (top). Histological verification of the virus injection within the LPO and optical fiber placements within the VTA is shown. Boundaries of the VTA are shown by tyrosine hydroxylase detection (TH; magenta) and eYFP shows LPO axons (green) (bottom).

(B) Timeline for the place conditioning procedure. Mice were tested for baseline preference, followed by four pairing sessions (Paired 1–4) and a stimulation-free test (Paired T1).

Subsequently, the paired compartment was reversed for four reversal sessions (Reversal 1–4) and a stimulation-free test (Reversal T2).

(C) VGluT2-ChR2 mice with VTA photostimulation of LPO-VGluT2 fibers spent less time in the chamber paired with photostimulation on conditioning days (blue line) and exhibited place aversion during stimulation-free test sessions (n = 14 mice). VGuT2-eYFP-mice with VTA photostimulation of LPO glutamate fibers spent equal times in the photostimulation paired and unpaired chambers (n = 7 mice) (generalized linear model; n = 21; chamber × session × group interaction, $\chi^2_{(20)} = 105.992$, p = 1.0503E—13; *p < 0.05; data represent the mean ± SEM).

(D) VGaT-ChR2 mice with VTA photostimulation of LPO-VGaT fibers spent more time in the photostimulation-paired chamber during conditioning (blue line) sessions without developing conditioned place preference for the photostimulation-paired chamber (n = 14 mice). VGaT-eYFP mice with VTA photostimulation of LPO-VGaT fibers did not show a preference for either the paired or the unpaired chamber (n = 7 mice). Data are shown as the mean ± SEM (generalized linear model; n = 21; chamber × session × group interaction, $\chi^2_{(20)} = 42.28$, p = 0.003; *p < 0.05). (See also Figure S2.) LPO, lateral preoptic area; MPO, medial preoptic area; VP, ventral pallidum; HDB, horizontal diagonal band; ac, anterior commissure; VTA, ventral tegmental area.

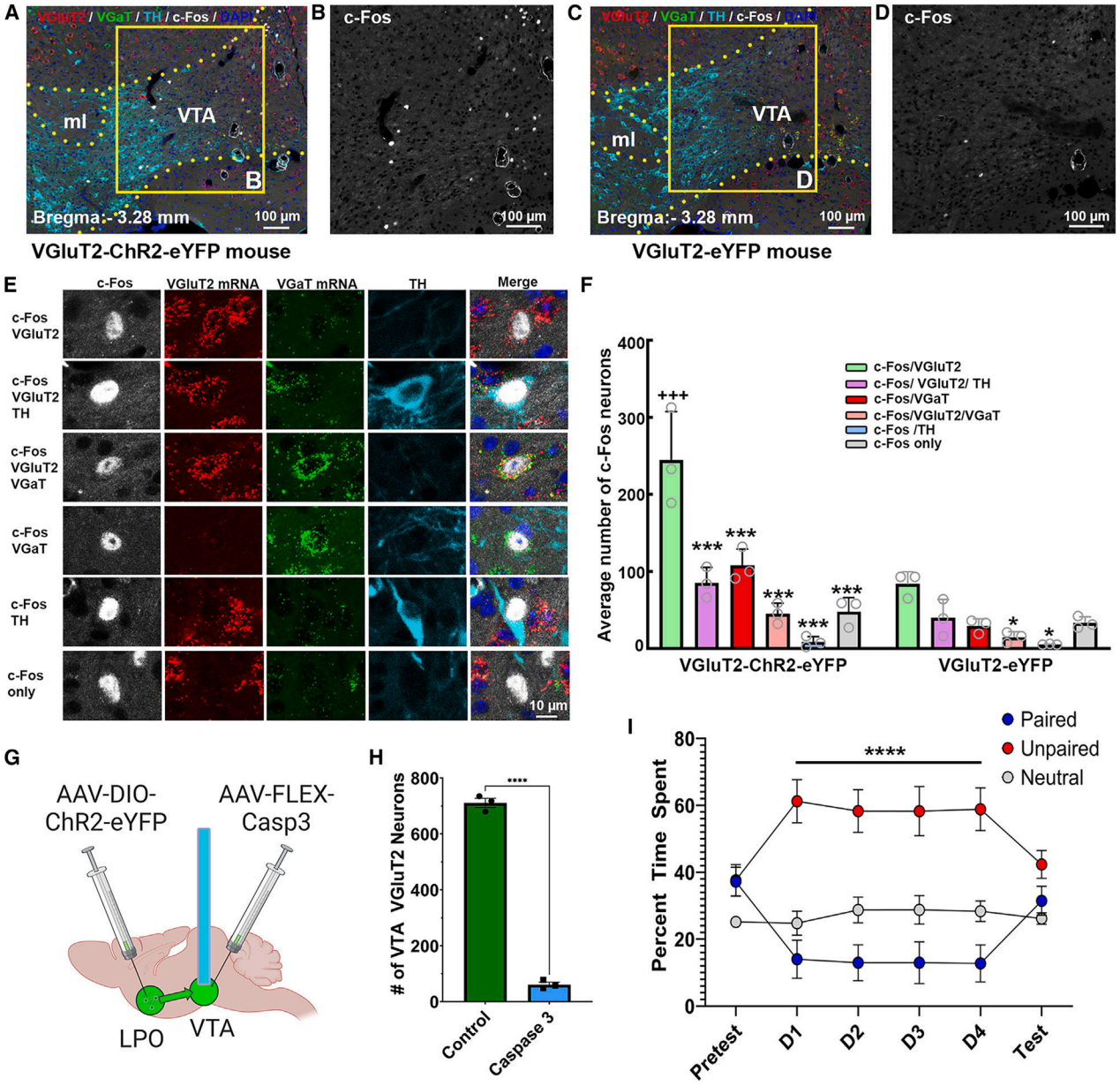

Figure 4. LPO glutamate inputs to the VTA signal aversion through non-glutamatergic neurons

(A–D) c-Fos expression (white nuclei) induced by VTA photostimulation of LPO VGluT2 fibers in naive VGluT2-ChR2-eYFP mice (A and B) or VGluT2-eYFP mice (C and D). VTA, ventral tegmental area; ml, medial lemniscus.

(E) Phenotype of c-Fos neurons. From top to bottom: neuron coexpressing c-Fos and VGluT2 mRNA (c-Fos/VGluT2); neuron coexpressing c-Fos, VGluT2 mRNA, and TH (c-Fos/VGluT2/TH); neuron coexpressing c-Fos, VGluT2 mRNA, and VGaT mRNA (c-Fos/VGluT2/VGaT); neuron coexpressing c-Fos and VGaT mRNA (c-Fos/VGaT); neuron coexpressing c-Fos and TH (c-Fos/TH); and neuron lacking VGluT2, VGaT, and TH (c-Fos only).

(F) The population of VTA neurons expressing c-Fos was higher in ChR2-eYFP mice (359.7 ± 11.3; n = 3, 15 sections/mouse) than in eYFP mice (206.0 ± 16.8; n = 3, 15 sections/mouse; $t_{(4)} = 16.49$, $p < 0.0001$, t test). Within the VTA of ChR2-eYFP mice, most c-Fos neurons coexpressed VGluT2 mRNA (245.00 ± 36.3; 735 neurons), some coexpressed VGluT2 and TH (85.33 ± 11.57; 256 neurons) or VGluT2 and VGaT (45.33 ± 7.80; 136 neurons) or VGaT (107.67 ± 12.44; 323 neurons), fewer coexpressed TH (8.33 ± 4.10, 25 neurons), and some lacked VGluT2, VGaT, and TH (48.00 ± 10.50, 144 neurons; cell type: $F_{(5,20)} = 29.07$, $p < 0.00001$, ANOVA with Newman-Keuls *post hoc* test). Significant difference from c-Fos/VGluT2 neuronal subtype: ***$p < 0.001$, *$p < 0.05$. Difference from eYFP mice: $^{+++}p < 0.001$.

(G) Diagram of virus injection (AAV5-EF1α-DIO-ChR2-eYFP) in the LPO and VTA (AAV1-FLEX-Casp3) for the VTA ablation of *vglut2* neurons and VTA photostimulation of LPO-VGluT2 fibers in VTA.

(H) The AAV encoding caspase 3 in the VTA reduced the number of VTA *vglut2* neurons ($t_{(4)} = 35.08$, ****$p < 0.0001$).

(I) Despite lesioning ~92% of VTA VGluT2 neurons, optogenetic stimulation of LPO-VGluT2 neurons innervating the VTA continued to drive aversion toward the paired chamber (chamber × session, $F_{(10, 144)} = 4.60$, $p < 0.0001$). Significant difference from unpaired chamber: ****$p < 0.001$; all data represent mean ± SEM.

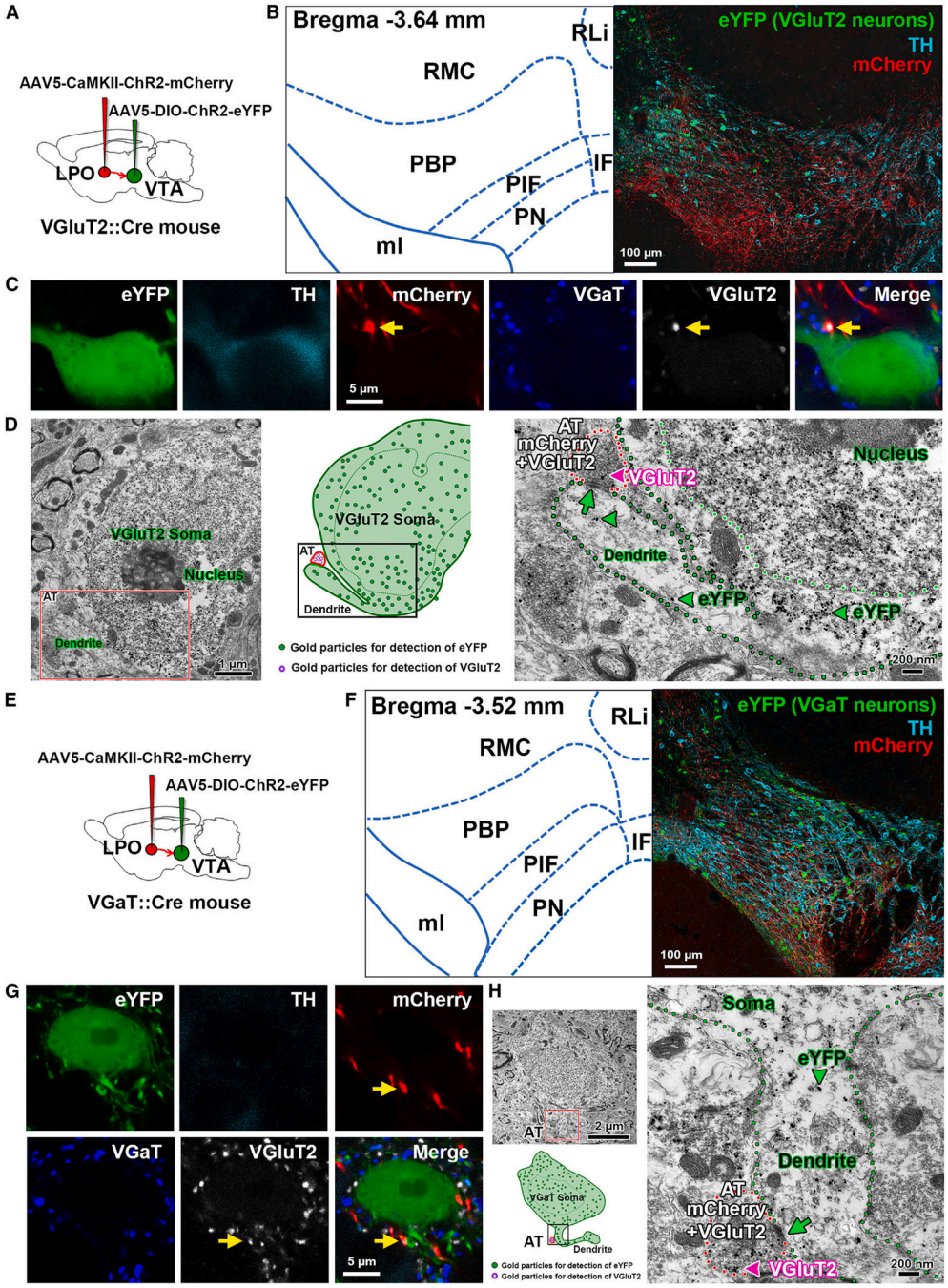

Figure 5. Axon terminals from the LPO VGluT2 neurons establish asymmetric synapses on VTA TH, VGluT2, or VGaT neurons

(A) Diagram of viral injection of AAV5-CaMKII-ChR2-mCherry into the LPO and AAV5-DIO-ChR2-eYFP into the VTA of *vglut2:cre* mice.

(B) Confocal micrograph of VTA at low magnification. TH, cyan; VGluT2-eYFP neurons, green; and mCherry fibers from LPO, red.

(C) Confocal micrographs at higher magnification showing the primary dendrite of a VTA TH and VGluT2-eYFP coexpressing neuron contacting an LPO-VGluT2 terminal coexpressing mCherry and VGluT2 protein (arrows).

(D) Electron micrographs and corresponding diagram showing a VGluT2 axon terminal (AT; red outlines) coexpressing mCherry (scattered dark material) and VGluT2 (pink arrowhead, gold particle) from an LPO neuron making an asymmetric synapse (green arrow) with the primary dendrite (green outline) of a VTA-VGluT2-eYFP neuron (eYFP detection by gold particles, green arrowheads).
(E) Diagram of viral injection of AAV5-CaMKII-ChR2-mCherry into the LPO and AAV5-DIO-ChR2-eYFP into the VTA of *vgat:cre* mice.
(F) Confocal micrograph of VTA at low magnification. TH, cyan; VGaT-eYFP neurons, green; and mCherry fibers from LPO, red.
(G) Confocal micrographs at higher magnification showing an LPO-VGluT2 terminal (coexpressing mCherry and VGluT2 protein, arrows) contacting the primary dendrite of a VTA VGaT-eYFP neuron.

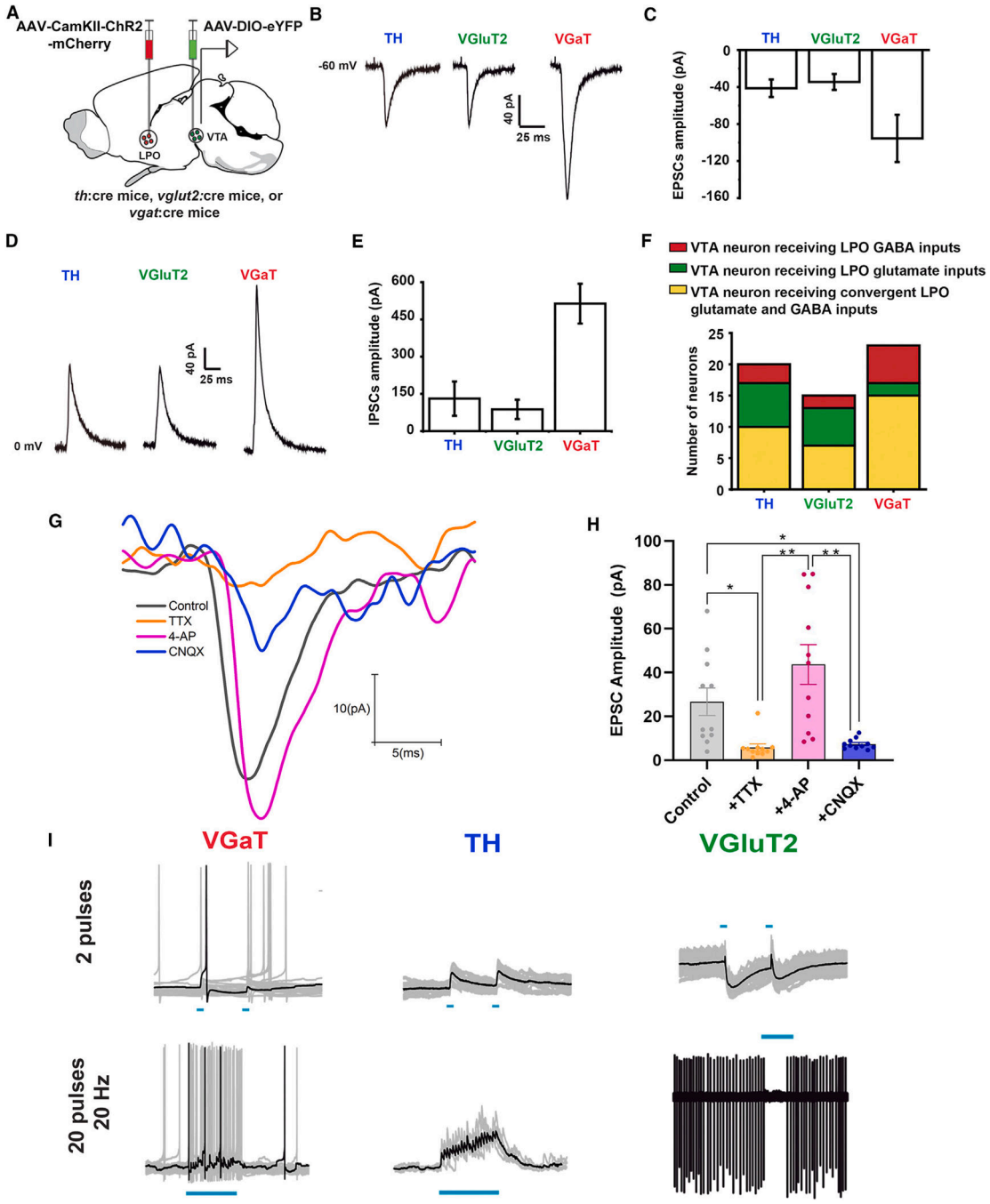

Figure 6. LPO neurons provide differential excitatory or inhibitory inputs to VTA-TH, VTA-VgluT2, and VTA-VGaT neurons

(A) Diagram of viral injection of AAV5-CAMKII-ChR2-mCherry into LPO and AAV5-DIO-eYFP into VTA of *th*:*cre*, *vglut2*:*cre*, or *vgat*:*cre* mice.

(B and C) VTA photostimulation of LPO inputs and voltage-clamp traces (B) and amplitude histogram (C) of isolated EPSCs recorded at −60 mV in VTA neurons (TH, VGluT2, and VGaT).

(D and E) VTA photostimulation of LPO inputs and voltage clamp traces (D) and amplitude histogram (E) of isolated IPSCs recorded at 0 mV in VTA neurons (TH, VGluT2, and VGaT).

(F) Histogram showing independent LPO excitatory, independent LPO inhibitory, and converging excitatory and inhibitory inputs on TH, VGluT2, and VGaT neurons.

G and H) Confirmation that LPO excitatory inputs to the VTA are monosynaptic. The perfusion of tetrodotoxin (TTX; 1 μM) decreased significantly (5.82 ± 1.61 pA) EPSCs (control, 26.68 ± 6.26 pA), and 4-AP (200 μM) recovered the amplitude of these currents (43.72 ± 9.09 pA). After the confirmation of the monosynaptic nature of the currents, the treatment with cyanquixaline (CNQX;10 μm) significantly decreased the glutamatergic currents (7.41 ± 0.71 pA) (treatment: $F_{(3,30)} = 14.08$, $p < 0.0001$).

(I) Current clamp traces of VTA neurons. VTA photoactivation of LPO inputs activates VTA-TH neurons and inhibits VTA-VGaT neurons (20 Hz pulses; 2 pulses top or 20 pulses bottom). *$p < 0.05$; **$p < 0.01$; all data represent mean ± SEM.

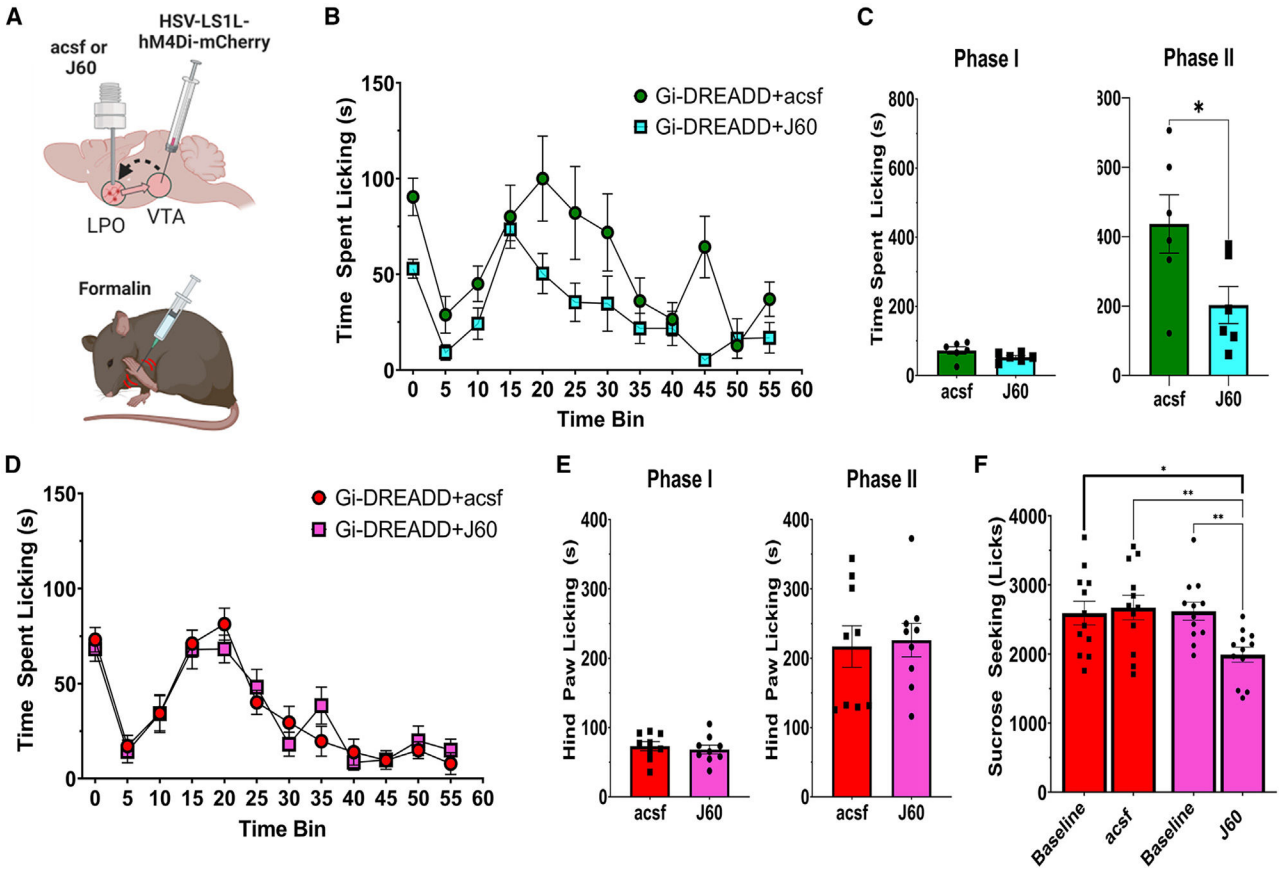

Figure 7. Inputs from LPO-VGluT2 neurons to VTA modulate the expression of pain

(A) Diagram of surgical procedures and formalin task. Retrograde Cre-dependent HSV-LS1L-hM4Di-mCherry viral vector was injected into the VTA of *vglut2:cre* or *vgat:cre* mice and a cannula implanted for intracranial injections of aCSF (control) or the hM4Di-DREADD agonist J60 (200 nL, 0.1 μg/mL) to inhibit LPO → VTA *vglut2* or *vgat* neurons.

(B and C) hM4Di inhibition of LPO-VGluT2 inputs to the VTA reduces hindpaw licking in phase II, but not phase I, of the formalin footpad test compared with aCSF controls (phase I, $t_{(10)} = 1.69$, $p = 0.12$; phase II, $t_{(10)} = 2.34$, $p = 0.04$).

(D and E) hM4Di inhibition of LPO-VGaT inputs to the VTA does not affect responses in either phase of the formalin footpad test (phase I, $t_{(16)} = 0.53$, $p = 0.60$; phase II, $t_{(16)} = 0.24$, $p = 0.81$).

(F) hM4Di inhibition of LPO-VGaT inputs to the VTA does produce a modest reduction in the consumption of a sucrose reward compared with both aCSF controls and a within-subjects baseline test for sucrose consumption (session × treatment, $F_{(1,11)} = 10.86$, $p = 0.0072$). *$p < 0.05$, **$p < 0.01$; all data represent mean ± SEM.

KEY RESOURCES

REAGENT or RESOURCE	SOURCE	IDENTIFIER
Antibodies		
Anti-Fluorogold	Millipore	Cat. # AB153; RRID AB_2314412
Biotinylated goat anti-rabbit	Vector Labs	Cat. # BA1000; RRID AB_2313606
Anti-cFos	Cell Signaling Technologies	Cat. # mAB5348; RRID:AB_10557109
anti-TH antibody	Millipore	Cat. # MAB318; RRID:AB_2201528
anti-Calbindin	Abcam	Cat. # ab156812; RRID:AB_2747594
anti-Substance-P	Neuromics	Cat. # P14103; RRID: AB_2629484
647 Alexa Fluor anti-mouse	Jackson ImmunoResearch Labs	Cat. # 71560517; RRID:AB_2338075
594 Alexa Fluor anti-guinea pig	Jackson ImmunoResearch Labs	Cat. # 706585148; RRID:AB_2340474
488 Alexa Fluor anti-rabbit	Jackson ImmunoResearch Labs	Cat. # 711545152; RRID:AB_2313584
405 Dylight anti-goat	Jackson ImmunoResearch Labs	Cat. # 705475147; RRID:AB_2340427
anti-mCherry	Takara	Cat. # 632543; RRID:AB_2307319
anti-VGluT2	Frontier Institute	VGluT2-Go-Af310; RRID: AB_2571620
Anti-VGaT	Frontier Institute	Cat# VGAT-GP, RRID:AB_2571624
anti-TH	Millipore	Cat. # AB152; RRID:AB_390204
DyLight-405-donkey anti-guinea pig	Jackson ImmunoResearch Labs	Cat# 706-475-148, RRID:AB_2340470
Alexa-Fluor-594-donkey anti-mouse	Jackson ImmunoResearch Labs	Cat# 715-585-151, RRID:AB_2340855
Alexa-Fluor-647-donkey anti-goat	Jackson ImmunoResearch Labs	Cat# 705-605-147, RRID:AB_2340437
Alexa-Fluor-750-donkey anti-rabbit	Abcam	Cat. # ab175731; RRID:AB_2943056
Bacterial and virus strains Titer		
AAV6-Syn-ChR2-eYFP	ViroVek	2-5e+13 vg/ml
HSV-hEF1 α-LS1L-GCaMP6s	Massachusetts General Hospital	5×10^9 vg/ml
AAV5-ef1 α-DIO-ChR2-eYFP	UNC Vector Core	5×10^{12} vg/ml
AAV5- ef1 α -DIO-eYFP-WPRE-PA	UNC Vector Core	5×10^{12} vg/ml
AAV5-CaMKII-ChR2(H134R)-mCherry	UNC Vector Core	5×10^{12} vg/ml
Experimental models: Organisms/strains		
VGaT-IRES-Cre	The Jackson Laboratory	Stock#: 016962; RRID:IMSR_JAX:016962
Vglut2-IRES-Cre	The Jackson Laboratory	Stock #: 016963, backcrossed onto C57Bl/6 at NIDA IRP; RRID:IMSR_JAX:016963
TH-Cre	International Mouse Strain Resource	MGI: 3056580
Software and algorithms		
Synapse	Tucker Davis Technologies	RRID:SCR_006495
Med PC IV	Med-Associates	N/A
MATLAB Scripts	MathWorks	https://github.com/djamesbarker/FiberPhotometry https://doi.org/10.5281/zenodo.5781801
Prism 8.0 & 9.0	GraphPad	RRID: SCR_002798
Adobe Creative Cloud	Adobe	RRID: SCR_014199